Cancer Cell

Article

Genome-wide CRISPR screens identify critical targets to enhance CAR-NK cell antitumor potency

Graphical abstract

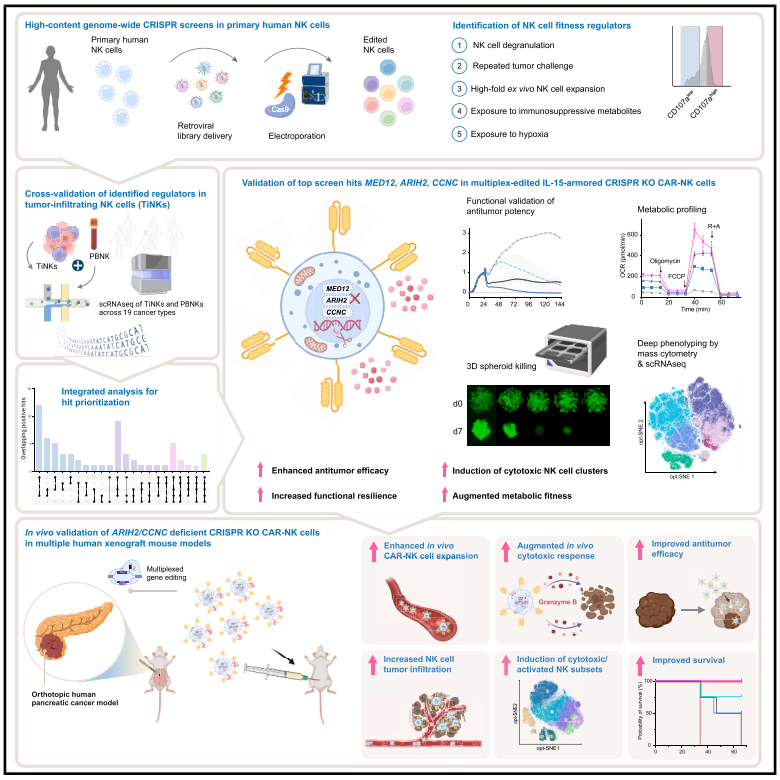

Authors

Alexander Biederstädt, Rafet Basar, Jeong-Min Park, ..., Natalie Wall Fowlkes, Ken Chen, Katayoun Rezvani

Correspondence

krezvani@mdanderson.org

In brief

Biederstädt et al. conduct genome-wide CRISPR screens in primary human NK cells, identifying *MED12*, *ARIH2*, and *CCNC* as critical regulators of antitumor activity. Targeted knockout of these genes enhances CAR-NK cell cytotoxicity, cytokine release, and metabolic fitness, providing a mechanistic framework for developing next-generation NK cell therapies against treatment-resistant malignancies.

Highlights

- Genome-wide CRISPR screens uncover critical regulators of NK cell function
- Orthogonal screens reveal targets to overcome NK cell dysfunction in the TME
- Knockout of *MED12*, *CCNC*, or *ARIH2* enhances NK cell antitumor potency
- Dual KO of *ARIH2* and *CCNC* in CAR-NK cells improves *in vivo* antitumor efficacy

Biederstädt et al., 2025, Cancer Cell *43*, 1–20
November 10, 2025
https://doi.org/10.1016/j.ccell.2025.07.021

CellPress

Please cite this article in press as: Biederstädt et al., Genome-wide CRISPR screens identify critical targets to enhance CAR-NK cell antitumor potency, Cancer Cell (2025), https://doi.org/10.1016/j.ccell.2025.07.021

Cancer Cell

CellPress
OPEN ACCESS

Article

Genome-wide CRISPR screens identify critical targets to enhance CAR-NK cell antitumor potency

Alexander Biederstädt,[1,2,3,8] Rafet Basar,[1,2,8] Jeong-Min Park,[1,2] Nadima Uprety,[1,2] Rejeena Shrestha,[1,2] Francia Reyes Silva,[1,2] Merve Dede,[4] John Watts,[1,2] Sunil Acharya,[1,2] Donghai Xiong,[1,2] Bin Liu,[1,2] May Daher,[1,2] Hind Rafei,[1,2] Pinaki Banerjee,[1,2] Ping Li,[1,2] Sanjida Islam,[1,2] Huihui Fan,[5] Mayra Shanley,[1,2] Jingling Jin,[1,2] Bijender Kumar,[1,2] Vernikka Woods,[1,2] Paul Lin,[1,2] Silvia Tiberti,[1,2] Ana Karen Nunez Cortes,[1,2] Xin Ru Jiang,[1,2,6] Inci Biederstädt,[1,2] Patrick Zhang,[1,2] Ye Li,[1,2] Seema Rawal,[1,2] Enli Liu,[1,2] Luis Muniz-Feliciano,[1,2] Gary M. Deyter,[1,2] Elizabeth J. Shpall,[1] Natalie Wall Fowlkes,[1,2,7] Ken Chen,[4] and Katayoun Rezvani[1,2,9,*]

[1]Department of Stem Cell Transplantation and Cellular Therapy, The University of Texas MD Anderson Cancer Center, Houston, TX, USA
[2]Institute for Cell Therapy Discovery and Innovation, The University of Texas MD Anderson Cancer Center, Houston, TX, USA
[3]Department of Medicine III: Hematology & Oncology, School of Medicine, Technical University of Munich, Munich, Germany
[4]Department of Bioinformatics and Computational Biology, The University of Texas MD Anderson Cancer Center, Houston, TX, USA
[5]Department of Neurology, the University of Texas McGovern Medical School at Houston, Houston, TX, USA
[6]The University of Texas MD Anderson Cancer Center UTHealth Houston Graduate School of Biomedical Sciences, Houston, TX, USA
[7]Department of Veterinary Medicine & Surgery, The University of Texas MD Anderson Cancer Center, Houston, TX, USA
[8]These authors contributed equally
[9]Lead contact
*Correspondence: krezvani@mdanderson.org
https://doi.org/10.1016/j.ccell.2025.07.021

SUMMARY

Adoptive cell therapy using engineered natural killer (NK) cells is a promising approach for cancer treatment, with targeted gene editing offering the potential to further enhance their therapeutic efficacy. However, the spectrum of actionable genetic targets to overcome tumor and microenvironment-mediated immunosuppression remains largely unexplored. We performed multiple genome-wide CRISPR screens in primary human NK cells and identified critical checkpoints regulating resistance to immunosuppressive pressures. Ablation of *MED12*, *ARIH2*, and *CCNC* significantly improved NK cell antitumor activity against multiple treatment-refractory human cancers *in vitro* and *in vivo*. CRISPR editing augmented both innate and CAR-mediated NK cell function, associated with enhanced metabolic fitness, increased secretion of proinflammatory cytokines, and expansion of cytotoxic NK cell subsets. Through high-content genome-wide CRISPR screening in NK cells, this study reveals critical regulators of NK cell function and provides a valuable resource for engineering next-generation NK cell therapies with improved efficacy against cancer.

INTRODUCTION

Allogeneic natural killer (NK) cells, engineered to express chimeric antigen receptors (CARs), have shown remarkable safety and efficacy in advanced hematologic malignancies.[1–4] However, their therapeutic potential remains constrained by limited persistence, functional exhaustion, and the immunosuppressive tumor microenvironment (TME), particularly in solid tumors. Overcoming these barriers necessitates a deeper understanding of the molecular regulators that govern NK cell fitness and anticancer immunity.[5] While previous studies have identified inhibitory checkpoints that can be targeted to enhance NK cell function,[6–18] the landscape of actionable genetic targets remains limited due to an incomplete understanding of NK cell-specific regulatory pathways.

Large-scale CRISPR screens in primary human T cells have identified regulators of antitumor immunity, offering a systematic approach to gene target discovery.[19–22] Similar studies in murine NK cells have identified key regulators of NK cell function[9]; however, genome-wide CRISPR screens in primary human NK cells have been hampered by technical challenges, including difficulties in editing NK cells at scales required to ensure adequate screen coverage.

Here, we report the development of a genome-wide CRISPR screening platform, optimized for primary human NK cells, enabling unbiased interrogation of gene programs that govern cytotoxicity, persistence, and resistance to suppression. Through high-content screens under repeated tumor challenge and immunosuppressive stress, we identified key regulators of NK cell dysfunction that can be targeted to enhance CAR-NK cell activity within the TME. Together, these findings provide a foundation for the development of next-generation NK cell therapies with improved efficacy against both hematologic and solid tumors.

Please cite this article in press as: Biederstädt et al., Genome-wide CRISPR screens identify critical targets to enhance CAR-NK cell antitumor potency, Cancer Cell (2025), https://doi.org/10.1016/j.ccell.2025.07.021

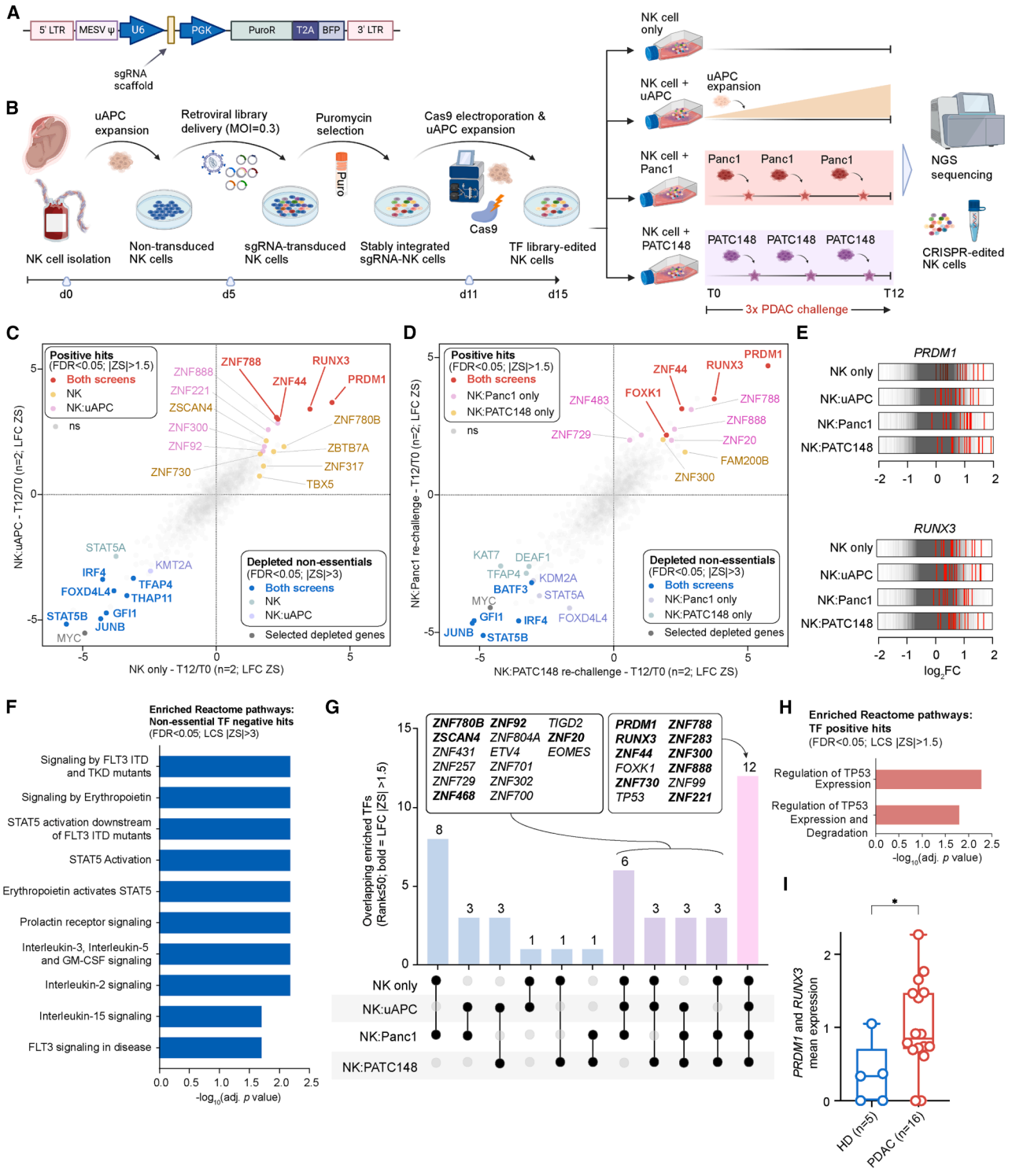

Figure 1. Pooled CRISPR screening in primary human NK cells enables massively parallel interrogation of genomic perturbations

(A) Conceptual of the sgRNA transfer plasmid used for retroviral library delivery (See also Figure S1).

(B) Schematic representing the gene editing pipeline for pooled CRISPR screening in primary human NK cells employed for the four targeted CRISPR knockout (KO) screens using a transcription factor (TF) sgRNA library.

(C and D) TF library CRISPR screens (targeting 1,632 genes with 11,364 unique sgRNAs) in primary human NK cells ($n = 2$ human CB donors) revealed shared and context-specific genes governing transcriptional regulation associated with NK cell function including under feeder cell-enabled high-fold *in vitro* expansion (C) and repeated pancreatic tumor challenge (D). Depicted are z-transformed $\log_2$ fold changes (LFC ZS) comparing relative sgRNA abundance at T12 vs. T0

(legend continued on next page)

Please cite this article in press as: Biederstädt et al., Genome-wide CRISPR screens identify critical targets to enhance CAR-NK cell antitumor potency, Cancer Cell (2025), https://doi.org/10.1016/j.ccell.2025.07.021

RESULTS

CRISPR discovery platform enables systematic interrogation of genetic perturbations in primary human NK cells

To enable pooled gene editing in primary human NK cells, we developed a retroviral vector system incorporating a guide RNA expression cassette (sgRNA scaffold) (Figure 1A). Cord blood (CB)-derived NK cells were expanded with engineered universal antigen-expressing feeder cells (uAPCs[23]) plus IL-2 (200 IU/mL), transduced with the sgRNA vector, electroporated with Cas9 protein and selected with puromycin while undergoing uAPC re-expansion (Figure S1A).

Extensive optimization was undertaken to ensure adequate editing efficiency and NK cell recovery post-electroporation. First, we evaluated the kinetics of retroviral sgRNA integration and the stability of GFP-labeled Cas9 protein following electroporation (Figures S1B and S1C). Next, we tested various pulse codes to determine optimal electroporation parameters for NK cells, with targeted ablation of the NK cell surface marker Protein Tyrosine Phosphatase Receptor Type C [*PTPRC* (CD45)] serving as readout (Figure S1D). Finally, NK cell viability and stable vector integration were confirmed following puromycin selection (Figure S1E). Flow cytometry confirmed efficient *PTPRC* KO with 90.1% ± 0.1% loss of CD45 expression versus 0% in Cas9 mock-electroporated controls not receiving a guide (Figure S1F).

These efforts resulted in PreCiSE, a high-throughput discovery platform for the **p**ooled **re**troviral library delivery and Cas9 electroporation **i**n primary human NK cells to enable **s**ystematic **e**xploration of genetic perturbations.

Transcription factor library screens

Despite the therapeutic potential of transcriptional modulation,[24–26] the functional roles of most DNA-binding transcription factors (TFs) in NK cells remain unexplored. Using a library targeting 1,632 TFs with 11,364 unique guide sequences, we systematically interrogated NK cell transcriptional regulation in multiple clinically relevant settings.

Primary human NK cells from two donors were transduced with the TF library (Figure 1B) to determine the impact of targeted TF disruption on NK cell proliferation, persistence and cellular fitness cultured in the presence or absence of feeder cells (Figure 1B, top right). Parallel tumor re-challenge screens with Panc1 and PATC148 human pancreatic cancer (PDAC) cells enabled identification of TFs regulating tumor-induced NK cell dysfunction (Figure 1B, bottom right). After 12 days of culture, relative sgRNA abundance was quantified by next-generation sequencing (NGS) (Figures 1C–1E; Table S1). The screen demonstrated uniform guide distribution and fidelity in library presentation with minimal sgRNA dropout (≤50 reads) and robust identification of essential genes (Figures S1G–S1R). The analysis revealed several known genetic dependencies critical for NK cell survival and proliferation, including *JUNB*, *IRF4*, *BATF3*, *STAT5A*, and *STAT5B* (Figures 1C, 1D, and S1S–S1W). Overrepresentation analysis of non-essential gene depletion highlighted interleukin signaling and JAK-STAT pathway activity in sustaining NK cell functionality (Figure 1F).

Conversely, our screens identified strong enrichment of multiple TFs that could be targeted to enhance NK cell fitness (Figures 1C–1E and S1S–S1V). The high correlation in gene-level dependencies across donors and consistent overlap of the top 50 most enriched genes across all four screens (Figures 1C, 1D, 1G, and S1S–S1V) suggest conserved TF networks that drive NK cell proliferation and resistance to tumor-induced dysfunction. Notably, enriched hits were strongly associated with regulators of TP53 (Figure 1H), suggesting that targeting tumor suppressor pathways may enhance NK cell function.

Among the top hits, PR/SET Domain 1 [*PRDM1*, also known as Blimp-1), emerged as a recurrent regulator across all four screen conditions (Figures 1C–1E and 1G). *PRDM1* knockdown has been shown to enhance IFNγ and TNFα production in NK cells, and its frequent inactivation in NK cell lymphoma underscores its role in suppressing NK cell proliferation.[27,28] Similarly, RUNX Family Transcription Factor 3 (*RUNX3),* a tumor suppressor implicated in IL-15-induced NK cell maturation,[29,30] was enriched across all screens, supporting a role in limiting NK cell proliferation and antitumor response (Figures 1C–1E and 1G). Analysis of single cell RNA sequencing (scRNA-seq) data from patients with pancreatic cancer (n = 16) showed elevated *PRDM1* and *RUNX3* expression in both tumor-infiltrating and circulating peripheral blood (PB)-NK cells compared to healthy donors (n = 5) (Figure 1I).[31] Together, our study identifies *PRDM1* and *RUNX3* as key transcriptional regulators of NK cell function that may be targeted to enhance antitumor activity.

across indicated screening conditions for both donors. Significantly enriched (FDR<0.05, LFC ZS>|1.5|) and depleted (FDR<0.05, LFC ZS>|3|) non-essential genes are labeled; color-coding indicates shared and screen-exclusive hits (See also Figure S1).

(E) Enrichment of individual sgRNAs targeting *PRDM1* and *RUNX3* depicted as $\log_2$ fold changes (FC) (T12/T0) across four CRISPR screen conditions (n = 2 human NK cell donors).

(F) Shown are the top 10 enriched Reactome pathways among significantly depleted non-essential genes (FDR<0.05, LFC |ZS|>3) delineating functional programs indispensable for NK cell survival and fitness. Essential genes specific for NK cells were determined by adjusting screen dropouts for inferred common essential genes (DepMap, Broad 24Q2 Public Dataset[43]).

(G) Overlap analysis (Upset plot) of top 50 most highly enriched TFs across investigated selective pressures. Bar height represents the number of overlaps; the bottom panel indicates the overlapping screening conditions. Identified targets with 3 and 4 overlaps are labeled; top hits (LFC ZS > 1.5) are indicated in bold. Significant screen hits without intersections are omitted (See also Figure S1).

(H) Enriched Reactome pathways among significantly enriched TF screen hits (FDR<0.05; |ZS|>1.5).

(I) Interrogation of single cell transcriptomes of tumor-infiltrating and circulating peripheral blood (PB)-NK cells from patients with pancreatic cancer (n = 16) compared to healthy donor controls (n = 5) investigating a gene signature comprising the top two overlapping screen hits (*PRDM1*, *RUNX3*). Data represented as box-and-whiskers plots; box limits represent quartiles (IQR), whiskers indicate minimum and maximum values, the horizontal solid line represents the median; *p < 0.05; Mann Whitney U Test). Also see Figure S1 and Table S1.

Please cite this article in press as: Biederstädt et al., Genome-wide CRISPR screens identify critical targets to enhance CAR-NK cell antitumor potency, Cancer Cell (2025), https://doi.org/10.1016/j.ccell.2025.07.021

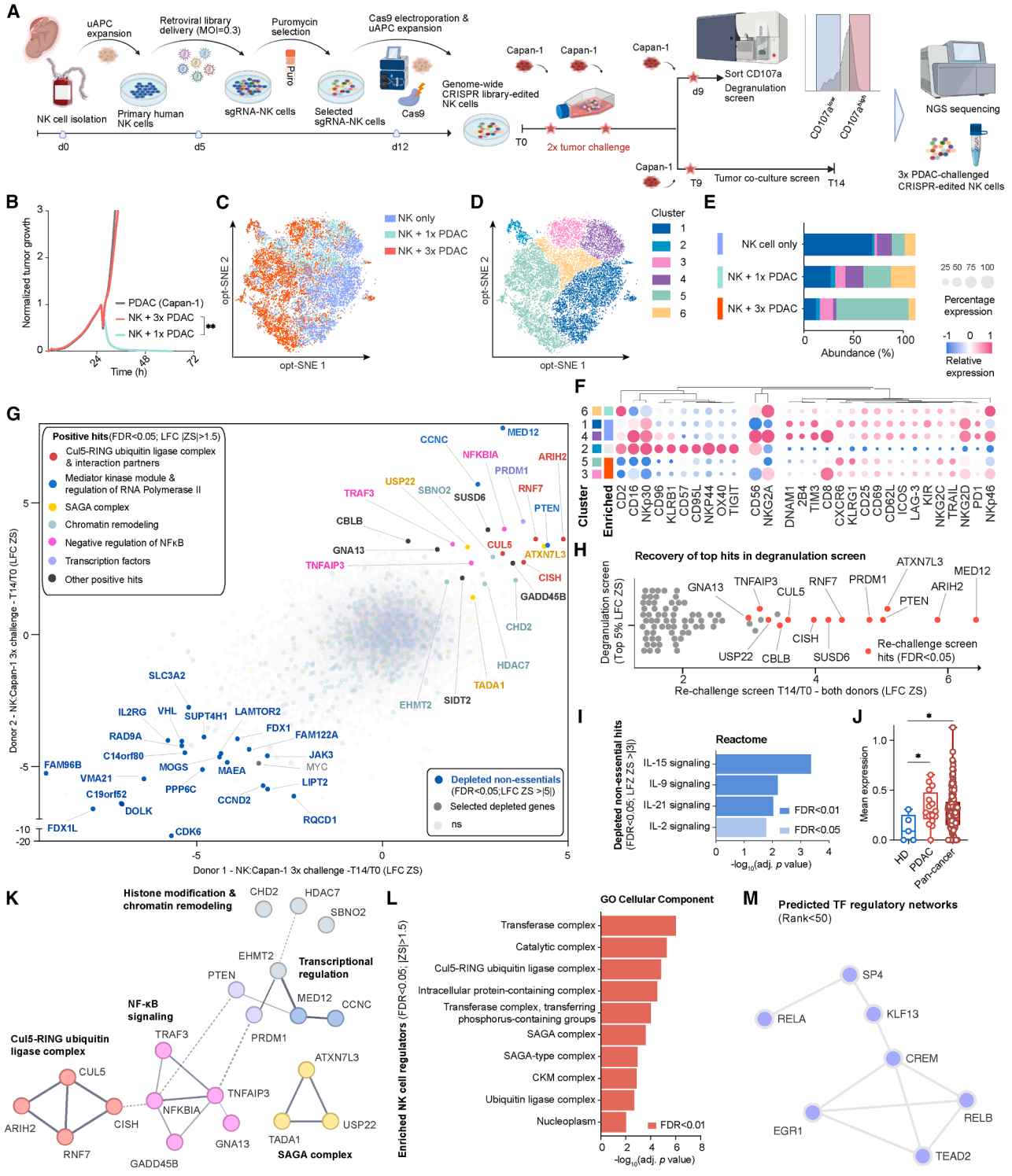

Figure 2. Genome-wide CRISPR screens in primary human NK cells decipher modulators mediating enhanced antitumor potency under repeated tumor challenge

(A) Schematic of high-content genome-wide CRISPR screens to identify regulators of NK cell functional resilience under repeated tumor pressure (See also Figure S2).

(B) NK cell:Capan-1 pancreatic cancer xCELLigence *in vitro* killing assay (E:T = 1:1) assessing NK cell antitumor potency after two rounds of Capan-1 tumor challenge (NK + 3x PDAC; red) compared to PDAC-naïve controls (NK + 1x PDAC; light green); shown is the mean normalized tumor growth of $n = 2$ independent

(legend continued on next page)

Genome-wide CRISPR screening enables unbiased interrogation of perturbations that enhance NK cell anticancer immunity

Systematic identification of gene targets that enhance NK cell fitness and function holds transformative potential, yet genome-wide perturbation studies in primary human NK cells have been limited by technical challenges. To address this, we developed a robust, genome-wide CRISPR screening platform for primary human NK cells. This included optimizing large-scale gene editing protocols to ensure efficient low-MOI transduction and high-coverage delivery of a 77,736 genome-wide sgRNA library, targeting 19,281 genes, with 500 non-targeting controls (Figures S1A–S1F and S2A). Primary human NK cells were transduced on day 5, puromycin-selected, electroporated with Cas9 protein and expanded with feeder cells plus IL-2 (Figure 2A, left).

NK cell activation and target engagement are governed by a complex array of germline receptors, making it difficult to rely on a single phenotypic marker to infer functional states. We therefore established a model of tumor-induced NK cell dysfunction by subjecting primary human NK cells to three sequential challenges with Capan-1 pancreatic cancer cells at an effector-to-target ratio (E:T) of 1:1. By the third tumor challenge (NK + 3x PDAC), NK cells displayed complete loss of tumor control, indicative of terminal functional exhaustion (Figures 2B and S2B). Multi-parameter spectral-flow cytometry revealed distinct phenotypic shifts with re-challenged NK cells (NK + 3x PDAC; red) clustering separately from non-challenged controls (NK only; blue) (Figures 2C and S2C–S2E). Dysfunctional NK cell clusters 3 and 5 ($CD16^{low}$, $NKp30^{low}$, $DNAM1^{low}$) increased after initial tumor challenge (NK + 1x PDAC; light green) and dominated following repeated re-challenges (NK + 3x PDAC), correlating with disappearance of functional $CD16^{high}$, $DNAM1^{high}$, $NKG2D^{high}$ NK cell clusters 1 and 4 (Figures 2D–2F and S2E). This model reliably induced sufficient functional differences for CRISPR-based readouts.

To conduct genome-wide CRISPR screens under tumor pressure, we subjected CRISPR library-edited NK cells to three rounds of challenges with Capan-1 cells starting on day 6 post-electroporation. After the third challenge, two parallel strategies were employed: (i) NK cells were sorted based on tail-end expression of the degranulation marker Lysosomal Associated Membrane Protein 1 [*LAMP1* (CD107a)] (Figure 2A, top right and S2F) or (ii) NK cells were cultured until day 14 to allow clonal outgrowth of cells with sgRNAs targeting inhibitory checkpoints (Figure 2A, bottom right). Genomic DNA was extracted from NK cells and subjected to deep sequencing to determine relative guide abundance.

Across the samples, the vast majority of library guides were retained with minimal dropouts (9–28 missed sgRNAs missed per sample, read count<50) (Figures S2G and S2H) and uniform sgRNA abundance across donors (Figures S2I–S2M). Gene-level abundance analyses revealed robust discrimination of essential genes (Figures S2N and S2O). By comparing abundance-based ranks between tumor-exposed NK cells and NK cells at T0, we identified sgRNAs that affected NK cell proliferation and persistence under tumor pressure as exemplified by strong enrichment of multiple‘ guides for two of the top screen hits, *MED12* and *PRDM1*, respectively (Figure S2P; Table S2).

Our genome-wide CRISPR screens identified both previously unrecognized and known regulators of NK cell function, including Cytokine Inducible SH2 Containing Protein *(CISH),* a checkpoint modulating IL-15 signaling*; PRDM1*, a transcription factor critical for NK cell identity and Phosphatase and Tensin Homolog (*PTEN*), a negative regulator of NK cell cytotoxicity (Figure 2G).[32] Hits were highly correlated between donors (Figure 2G). Moreover, top hits identified in the tumor re-challenge screens were enriched among the top 5% of hits in the degranulation screens (FDR<0.05; LFC |ZS|>1.5), pointing to shared regulatory networks underlying NK cells degranulation and cellular fitness under repeated tumor challenge (Figure 2H). Similarly, top hits from the TF library screens (rank<50; ≥2 overlaps) were significantly enriched among genes conferring a cell fitness advantage in the genome-wide NK cell tumor re-challenge screens (Figure S2Q). Conversely,

human NK cell donors. Error bars (SD) are represented as shaded area (*p* value computed using ratio paired t test of the reciprocal of the area under the tumor growth curve; $^{**}p < 0.01$; see also Figure S2B for AUC statistics).

(C and D) Optimized t-Distributed Stochastic Neighbor Embedding (opt-SNE) plots depicting NK single cell projections before (NK only; blue) and after one (NK + 1x PDAC; green) or three (NK + 3x PDAC; red) rounds of Capan-1 pancreatic cancer (PDAC) challenge (E:T = 1:1) (C), and overlaid with FlowSOM metaclusters (D), as assessed by spectral flow cytometry; $n = 2$ CB donors (See also Figures S2C–S2E).

(E) Bar chart depicting the changes in relative cluster composition across the different experimental groups ($n = 2$ human NK cell donors).

(F) Heatmap of z-transformed median surface marker expression (indicated by color) and percentage expression (indicated by circle size) for metaclusters. Columns are clustered using 1-Pearson correlation distance and average linkage.

(G) Genome-wide CRISPR screens in primary human NK cells ($n = 2$ donors) identifying positive (FDR<0.05; LFC |ZS|>1.5) and negative (FDR<0.05; LFC |ZS|>5) regulators of NK cell fitness under repeated pancreatic cancer challenge. Hits color-coded by molecular function and cellular localization (See also Figure S2).

(H) Integrated analysis of the genome-wide NK cell degranulation and NK:Capan-1 re-challenge screens reveals recovery of the majority of screen hits (FDR<0.05) identified in the NK cell re-challenge screen among top enriched genes ($\geq 95^{th}$ quantile LFC ZS) in the NK cell degranulation screens.

(I) Reactome pathway analysis of significantly depleted non-essential genes (FDR<0.05; LFC ZS>|3|).

(J) Single-cell transcriptomic data of tumor-infiltrating and peripheral blood (PB)-NK cells in pancreatic cancer ($n = 16$) and across 19 cancer types ($n = 217$), evaluating a gene signature comprising the top 5 hits compared to healthy controls ($n = 5$). Data represented as box-and-whiskers plots; box limits represent quartiles (IQR), whiskers indicate minimum and maximum values, horizontal solid line represents the median; *p* values computed using Mann-Whitney U test; $^{*}p < 0.05$ (See also Figures S2S and S2T).

(K) Genome-wide screens in primary human NK cells independently identified multiple components of integral cellular regulatory nodes as projected by protein-protein interaction mapping of screen hits (FDR<0.05) by STRING database.

(L) Gene ontology (GO) term analysis of positive hits (FDR<0.05, LFC ZS > 1.5) delineates cellular localization and functional context (See also Figures S2W and S2X).

(M) Top enriched hits (rank≤50) were analyzed using TRANSFAC and JASPAR databases to identify TF binding motifs and infer regulatory networks with shared binding to promoter regions of identified screen hits. Also see Figure S2 and Table S2.

Please cite this article in press as: Biederstädt et al., Genome-wide CRISPR screens identify critical targets to enhance CAR-NK cell antitumor potency, Cancer Cell (2025), https://doi.org/10.1016/j.ccell.2025.07.021

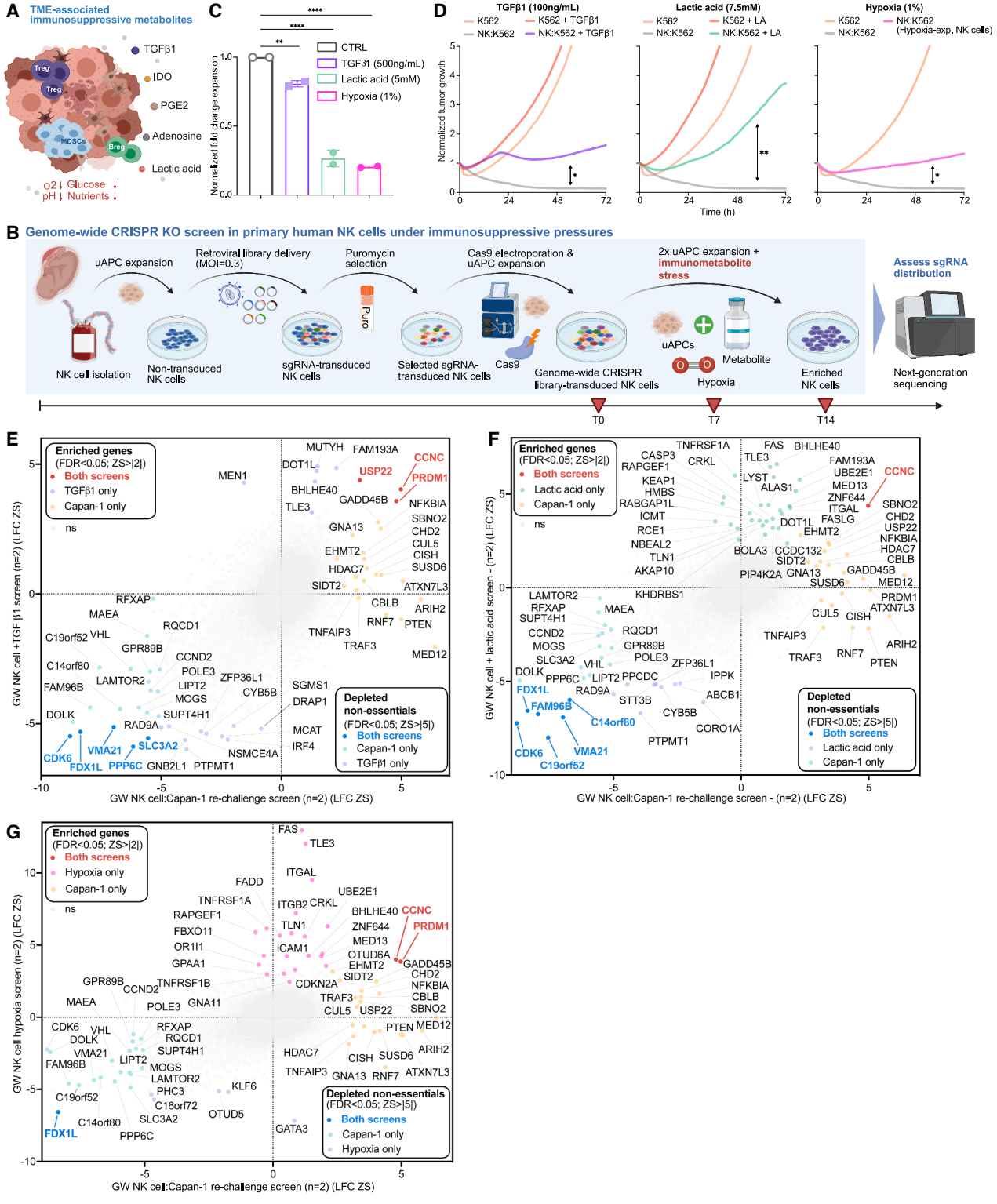

Figure 3. Genome-wide CRISPR screens in primary human NK cells identify targets shielding NK cells from immunosuppressive pressures in the TME

(A) Schematic portraying the immunosuppressive pressures encountered by tumor-infiltrating NK cells in the TME.

(B) Conceptual depicting the genome-wide CRISPR screen pipeline to systematically identify immunosuppressive resistance targets.

(legend continued on next page)

Please cite this article in press as: Biederstädt et al., Genome-wide CRISPR screens identify critical targets to enhance CAR-NK cell antitumor potency, Cancer Cell (2025), https://doi.org/10.1016/j.ccell.2025.07.021

bottom hits (non-essential genes; FDR<0.05; LFC |ZS|>3; ≥2 overlaps) were depleted (Figure S2R).

Our genome-wide CRISPR screens also uncovered positive regulators essential for NK cell activity. Among these, interleukin-2 receptor subunit gamma (*IL2RG*), a critical component of IL-2 and IL-15 receptors, and *janus kinase* 3 (*JAK3*), a member of the JAK/STAT signaling pathway, were significantly depleted in our screens, underscoring their indispensable roles in maintaining NK cell functionality (Figure 2G). Consistent with findings from our TF library screens, overrepresentation analysis of depleted non-essential genes in our genome-wide screens revealed strong enrichment for multiple interleukin signaling pathways (Figure 2I).

Validating screen hits using publicly available datasets

To confirm the clinical relevance of identified genes, we analyzed publicly available scRNA-seq datasets from NK cells of patients with pancreatic cancer. The gene signature from the top 5 hits in the Capan-1 re-challenge screens was significantly upregulated in tumor-infiltrating and circulating NK cells from pancreatic cancer patients compared to NK cells from healthy donors (Figure 2J).[31] Expanding this analysis across 19 diverse cancer types (n = 217 patients) revealed significant upregulation of this gene signature, highlighting the potential of identified hits as pan-cancer regulators of NK cell dysfunction (Figures 2J, S2S, and S2T).[31] Comparisons between tumor-infiltrating NK cells (TiNKs) and those from adjacent normal tissue demonstrated consistent upregulation across different solid cancers (Figure S2U).[31] Similarly, bone marrow-derived NK cells from patients with acute myeloid leukemia (AML; n = 8) showed marked upregulation of top screen hits versus healthy controls (n = 8), supporting their translational value as biomarkers of NK cell dysfunction and potential therapeutic targets (Figure S2V).[33]

Mapping regulatory nodes for NK cell reprogramming

To elucidate the molecular functions and localization of key hits from our NK cell tumor re-challenge screens, we performed protein-protein interaction mapping using the STRING database and GO term analysis of the top hits (FDR<0.05; LFC |ZS|>1.5) (Figures 2K and 2L). Enriched biological processes included pathways involved in transcriptional regulation, epigenetic modulation, and post-translational modification (Figures 2K, 2L, S2W, and S2X). Regulatory nodes included the Cdk8 kinase module (CKM) of the mediator complex, an evolutionarily conserved protein complex involved in regulating gene expression, the Spt-Ada-Gcn5 acetyltransferase (SAGA) complex, another conserved eukaryotic transcriptional co-activator complex, and the Cul5-RING-Ubiquitin ligase (CRL) complex. The CRL complex, which shapes NK cell functional states through interaction with SH2 domain-containing SOCS-box family proteins (CIS, SOCS1-7), includes high-ranking hits such as *CISH* and *SOCS1*[10,11,17,34–37] (Figure 2G; Table S2). Cul5, RBX2 (*RNF7*) and *ARIH2* (all high-ranking hits) act as scaffolds or accessory factors that facilitate substrate ubiquitylation and proteasomal degradation (Figures 2G and 2K). Another pathway linked to enhanced NK cell potency involved disruption of NF-κB antagonists, including *NFKBIA*, a subunit of the inhibitory IKK complex[38] (Figures 2G and 2K). Recent evidence positions *NFKBIA* as a potential checkpoint, with elevated expression in inflamed tumor-infiltrating NK cells.[31] Its disruption therefore removes a key brake on NF-κB activity, driving heightened NK cell effector functions.

To infer transcription factors potentially regulating these nodes, we examined binding motifs and uncovered several previously established master regulators of immune cell functional states, including the cAMP responsive element modulator (*CREM*), which we recently demonstrated to enhance CAR-NK cell efficacy (Figure 2M).[39]

Genome-wide CRISPR screens in primary human NK cells reveal targets to overcome TME-induced immunosuppression

NK cells encounter a complex array of immunosuppressive cues within the TME, which severely compromise their cytotoxic potential (Figure 3A). To decipher NK cell-intrinsic networks that process these inhibitory cues, we adapted our genome-wide CRISPR platform to identify genetic regulators of TME-induced dysfunction (Figure 3B). We screened NK cells under multiple immunosuppressive conditions, including transforming growth factor β (TGFβ), L-(+)-lactic acid, ammonium chloride (NH_4Cl), itaconic acid ($C_5H_6O_4$), hypoxia and dexamethasone, all of which variably suppressed NK cell cytotoxicity and proliferation (Figures 3C, 3D, and S3A–S3F). We performed orthogonal genome-wide CRISPR screens in primary human NK cells, applying immunosuppressive pressure while simultaneously driving their expansion with feeder cells and IL-2 (Figure 3B). This approach revealed both known and previously unknown regulators of NK cell function under TME-like conditions (Figures 3E–3G). Many of these were also detected in the Capan-1 tumor re-challenge screens (Figures S3G–S3J), underscoring their conserved role in mediating NK cell resistance across diverse challenges. The high-content screening

(C) Expanding primary human NK cells in the presence of transforming growth factor β1 (TGFβ1; 500ng/mL), L(+) lactic acid (5mM) or hypoxic stress (1% O2) severely blunts NK cell proliferation compared to metabolite-free controls (data presented as fold change expansion, T19 NK cell counts normalized to T13; mean ± SD of n = 2 human NK cell donors; $^{**}p < 0.01$, $^{****}p < 0.0001$; one-way ANOVA followed by Dunnett's test) (See also Figure S3B).

(D) NK cell cytotoxicity as assessed by Incucyte *in vitro* killing assays against K562 targets ± different immunosuppressive pressures including transforming growth factor β1 (TGFβ1; 100ng/mL), L(+) lactic acid (7.5mM) or previous expansion under hypoxic conditions (1% O2). (n = 2 human NK cell donors; mean (line) ±SD (shaded in gray); p values computed for the normalized NK cell killing capacity as assessed by one minus scaled area under the tumor growth curve using one-way ANOVA; $^{*}p < 0.05$, $^{**}p < 0.01$; K562 killing for metabolite-challenged NK cells was normalized to NK cell killing under normal conditions; see also Figures S3C–S3F).

(E–G) Enriched NK cell regulators and depleted non-essential genes across multiple immunosuppressive pressure screens (500ng/mL TGFβ1, 5mM L(+) lactic acid and 4% hypoxia) and the NK:Capan-1 re-challenge screens. Shown are z-transformed log2 fold changes (LFC ZS) of relative guide abundance at T14 vs. T0. Significantly enriched top hits (FDR<0.05, LFC ZS>|2|) and depleted non-essential gene programs (FDR<0.05, LFC ZS>|5|) are labeled and color-coded according to their overlap/exclusivity across indicated screen conditions. Shared hits between the genome-wide TME immunosuppression screens and the Capan-1 re-challenge screens are indicated in bold (n = 2 independent human NK cell donors). Also see Figure S3.

Please cite this article in press as: Biederstädt et al., Genome-wide CRISPR screens identify critical targets to enhance CAR-NK cell antitumor potency, Cancer Cell (2025), https://doi.org/10.1016/j.ccell.2025.07.021

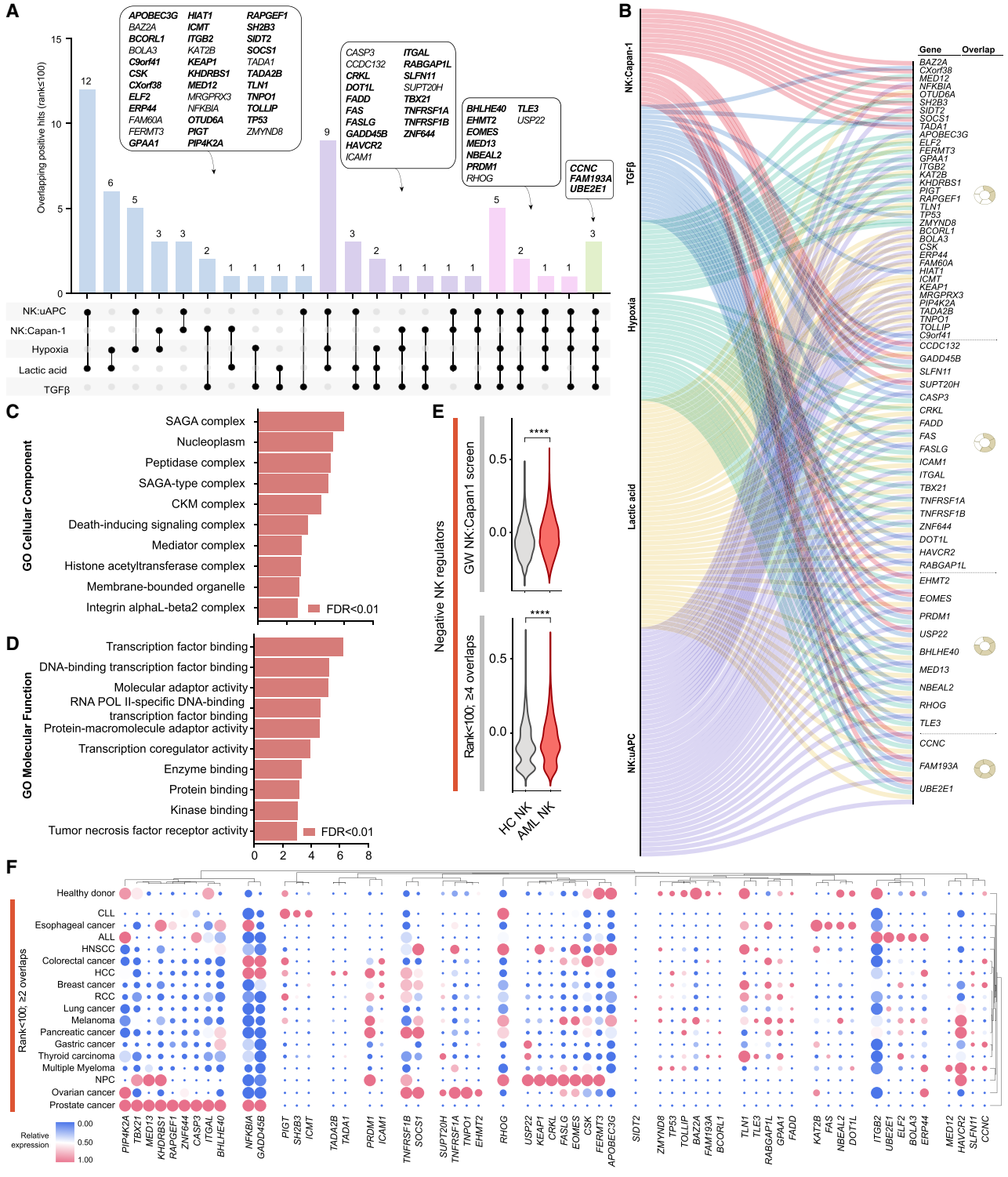

Figure 4. Integrated analysis reveals shared targets shielding NK cell from diverse clinically relevant pressures

(A) Top shared screen hits (rank≤100) across 5 genome-wide CRISPR KO screens in primary human NK cells with 2 (blue), 3 (purple), 4 (pink) and 5 (green) overlaps. Bar height represents the number of shared targets across screens indicated by dots in the lower panel. Enriched genes with LFC ZS > 2 in all screens labeled in bold. Significant screen hits without intersections are omitted (n = 2 human CB donors).

(B) Shared NK cell targets modulating resistance against multiple selective pressures including pancreatic cancer re-challenge (NK:Capan-1), TME-induced immunosuppression (TGFβ1, hypoxia, lactic acid) and *ex vivo* feeder cell-enabled high-fold expansion (NK:uAPC).

(C and D) Cellular localization and functional annotation of shared top hits (Rank≤100, ≥2 overlaps) by gene ontology (GO) term analysis.

(legend continued on next page)

Please cite this article in press as: Biederstädt et al., Genome-wide CRISPR screens identify critical targets to enhance CAR-NK cell antitumor potency, Cancer Cell (2025), https://doi.org/10.1016/j.ccell.2025.07.021

approach maintained exceptional quality under immunosuppressive conditions. Deep sequencing revealed minimal loss of sgRNAs (range: 9–36 missed sgRNAs; sgRNA read count <50) in harvested NK cells (Figure S4A). Guide distribution remained uniform (Figure S4B), and gene-level abundance-based ranking confirmed adequate discrimination of essentials genes (Figures S4C–S4F). Moreover, donor-to-donor correlation of gene-level data were strong (Figures S4G–S4J), and the results recapitulated NK cell regulators identified in our TF library screens (Figures S4K–S4R).

Modulating resistance to TGFβ

Overcoming TGFβ-mediated suppression, a key immunosuppressive factor in the TME, is critical for unlocking the full therapeutic potential of adoptively transferred NK cells. Using the PreCiSE platform, we identified several previously unrecognized modulators of TGFβ resistance (Figures 3E and S3G). Our screens underscored the known molecular redundancy of TGFβ signaling and ligand-receptor promiscuity in extracellular TGFβ sensing (Figure S4S).[40,41] Specifically, genomic loss of individual TGFβ receptor family members (e.g., *TGFBR2*: LFC ZS in 89.1st percentile) provided only a partial competitive advantage, even under overwhelming levels of TGFβ stress (500ng/mL). In contrast, ablation of downstream components of the TGFβ signaling pathway showed much stronger selection, with *SMAD2* and *SMAD4* ranking among the top 30 most enriched hits (Figure S4S).

Overcoming acidity-induced immunosuppression

Acidity within the TME, driven by lactic acid accumulation, may lead to therapeutic failure of adoptive cell therapies due to immune cell anergy.[42] We performed genome-wide CRISPR screens in primary human NK cells exposed to L(+)-lactic acid (5mM) and identified regulatory circuits that shield NK cells from low pH (Figures 3F and S3H). Positive hits (rank<100) included genes involved in acidity sensing (*GPI*, *TOLLIP*, and *ITGB2*) and modulating metabolic processes (*BHLHE40, ALAS1, PEPD, EHMT2, AKAP10, PIP4K2A, ALAD,* and *PCGF5*) (Table S2), highlighting metabolic reprogramming as a powerful means to enhance NK cell fitness within the TME.

Tuning NK cells to resist hypoxia

The hypoxic microenvironment of solid tumors poses another critical challenge to immune cell function. To uncover regulators of NK cell adaptation to low oxygen, we conducted genome-wide CRISPR screening at 4% O2 and identified multiple targets that impair NK cell function under hypoxia (Figures 3G and S3I; Table S2). Top-ranking hits (rank<100) included HIF-1α-regulated genes involved in metabolism (*UCP3*), apoptosis (*CASP3*, *FASLG*, and *FADD*), and migration (*ITGAL*, *ITGB2*, and *ICAM1*) (Table S2). Notably, HIF-1α-induced targets (e.g., *CORO1A*, *DOLK*, *CHUK*, and *AMD1*) were depleted in the hypoxia screens while HIF-1α-repressed targets (e.g., *LOX*, *CITED2*, and *HLA-DRB1*) were enriched (Figures S4T and S4U), suggesting that reinforcing HIF-1α–suppressed transcriptional programs augments NK cell fitness under hypoxic stress.

Genome-wide CRISPR screens nominate hits to augment NK cell fitness for clinical manufacturing

Donor-derived NK cell therapeutics require *ex vivo* expansion with engineered antigen-presenting cells and IL-2 to reach clinical doses. Although current protocols yield highly activated NK cells, prolonged culture may cause premature exhaustion and reduce therapeutic potency. To identify genetic perturbations that improve NK cell fitness during and after manufacturing, we performed genome-wide CRISPR knockout screens in ex vivo-expanded primary human NK cells. The screens revealed several key modulators including mediator complex components (*CCNC*, *MED12*, *MED13*, and *MED15*), apoptosis regulators (*FAS*, *TNFRSF1A*, and *SLFN11*), transcription factors (*AIP*, *BHLHE40*), ubiquitination regulators (*USP22*, *UBE2E1*, and *KEAP1*), and integrins (*ITGAL* and *ICAM1*), many of which overlapped with hits from tumor re-challenge and immunosuppression screens (Figures S3G–S3J; Table S2). These findings provide a roadmap for targeted gene-editing strategies to mitigate manufacturing-induced stress and improve of NK cell therapeutic quality.

Integrated analysis identifies conserved modulators of NK cell fitness

To identify gene targets with broad translational relevance, we integrated results from our TME pressure, NK cell expansion, and tumor re-challenge CRISPR screens, generating a comprehensive atlas of genetic perturbations conferring resistance to diverse immunosuppressive conditions (Figures 4A and 4B). Across five independent genome-wide screens in primary NK cells from two independent donors, we identified conserved hits regulating critical processes, including apoptosis (*CCNC*, *GADD45B*, *FAS*, *FASLG*, and *CASP3*), transcription (*PRDM1*, *BHLHE40*, *EOMES*, *DOT1L*, *MED13*, *ELF2*, *EHMT2*, *ZMYND8*, and *TLE3*), NF-κB signaling (*NFKBIA*), signal transduction (*CRKL*, *KHDRBS1*, *NBEAL2*, and *RHOG*), and ubiquitination (*UBE2E1* and *USP22*) (Figures 4A–4D).

Single-cell transcriptomes from cancer patients validated these findings. Genes from the NK cell tumor re-challenge screens (FDR<0.05; LFC |ZS|>1.5; Figure 4E, top)[33] and overlapping hits (rank ≤100) identified across ≥4 screens were significantly upregulated in NK cells from AML patients compared to healthy donors (Figure 4E, bottom).[33] Overlapping hits (rank

(E) Expression of significantly enriched targets (FDR<0.05; LFC |ZS|>1.5) from the genome-wide CRISPR tumor re-challenge screen (top) and overlapping screen hits (rank<100; ≥4 overlaps; bottom) in bone marrow-isolated primary human NK cells from patients with AML and healthy controls (n = 8 healthy human NK cell donors and n = 8 donors with AML; ****p < 0.0001; Mann-Whitney U test).

(F) Heatmap depicting the z-transformed relative expression of overlapping enriched screen hits (rank<100; ≥2 overlaps across 5 genome-wide CRISPR screens in primary human NK cells) in tumor-infiltrating NK cells (TiNKs) across 17 cancer types compared to healthy donor peripheral blood (PB) NK cells as surveyed by scRNA-seq data. Healthy donor (n = 5); CLL, chronic lymphocytic leukemia (n = 1); esophageal cancer (n = 11); ALL, acute lymphocytic leukemia (n = 2); HNSCC, head and neck squamous cell carcinoma (n = 33); colorectal cancer (n = 15); HCC, hepatocellular carcinoma n = 8); BC, breast cancer (n = 39); RCC, renal cell carcinoma (n = 27); lung cancer (n = 54); melanoma (n = 10); pancreatic cancer (n = 18); gastric cancer (n = 10); thyroid cancer (n = 9); multiple myeloma (n = 8); NPC, nasopharyngeal carcinoma (n = 10); ovarian cancer (n = 2); prostate cancer (n = 1). Color and circle size indicate z-transformed pseudobulk expression per gene. Also see Figure S5.

Please cite this article in press as: Biederstädt et al., Genome-wide CRISPR screens identify critical targets to enhance CAR-NK cell antitumor potency, Cancer Cell (2025), https://doi.org/10.1016/j.ccell.2025.07.021

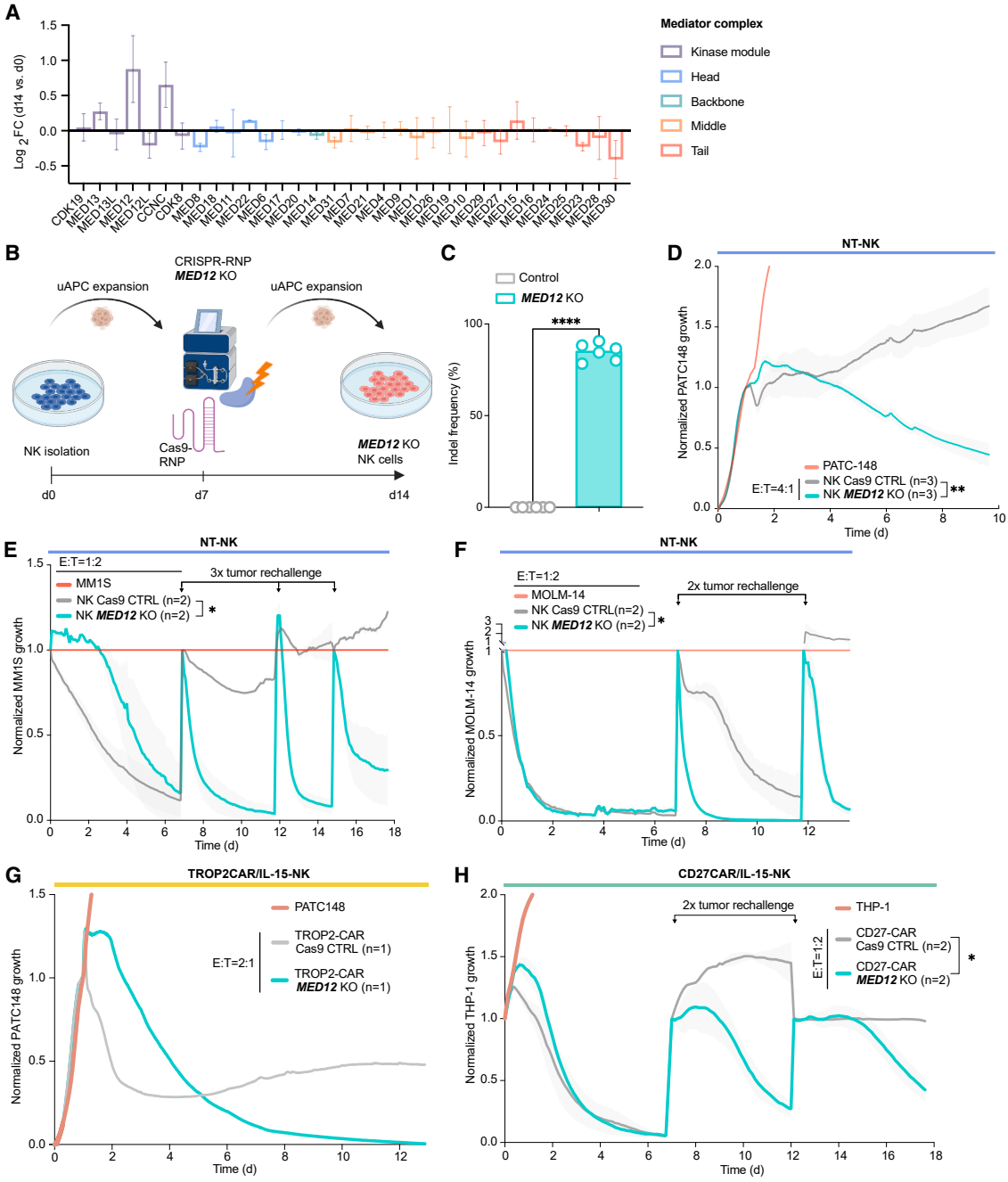

Figure 5. *MED12* ablation confers exhaustion resistance and tunes NK cells for enhanced antitumor function

(A) Mediator complex essentiality signature showing mean log2 fold-change (±SD) in sgRNA abundance from genome-wide NK cell Capan-1 re-challenge screens (n = 2 CB donors). Functional domains are color-coded.

(B) Schematic depicting the CRISPR-RNP-mediated disruption of the Mediator complex kinase module (CKM).

(C) *MED12* editing efficiency in CRISPR-RNP-edited NK cells measured by indel frequency (Tracking of Indels by DEcomposition [TIDE][67]; n = 6 CB donors; ****$p < 0.0001$, paired t-test) compared to mock controls.

(D) NK cell killing of PATC148 pancreatic cancer cells upon *MED12* deletion assessed by xCELLigence assay (n = 3 CB donors; mean normalized PATC148 tumor growth ±SD (shaded in gray); **$p < 0.01$ for the reciprocal of the scaled area under the tumor growth curve for corresponding donors, unpaired t-test; AUC summary statistics in Figure S7A).

(legend continued on next page)

≤100; ≥4 overlaps) also showed context-dependent induction in TiNKs across various cancer types compared to healthy donor-derived NK cells (Figure 4F).[31]

Conversely, genes consistently depleted across all five genome-wide screens (FDR<0.05) regulated immune response (*IRF4*, *TRAF1*), cell cycle (*CDK6, PPP6C*), cellular respiration (*COX11* and *FDX1L*), and metabolism (*LIPT2, DOLK, MOGS, PPCDC,* and *SEPHS2)* (Figure S5A).[43] Positive regulators were involved in chromatin remodeling (*CHRAC*), DNA replication (*POLE*) (Figures S5B–S5D) and were upregulated in NK cells from healthy donors compared to those from AML (Figure S5E, left)[33] or other cancer patients (Figure S5E, right).[31] These findings underscore the importance of epigenetic plasticity, DNA repair and metabolic fitness in sustaining NK cell function under immunosuppressive pressure.

Shared regulatory circuits across immune cell compartments

To assess the conservation of NK cell regulators across immune subsets, we integrated our findings with published CRISPR KO screens in primary human T and CAR-T cells (Figures S6A–S6D). This cross-lineage comparison revealed shared functional checkpoints (*MED12*, *CCNC*, *CBLB*, *TNFAIP3*, *ARIH2*, and *FAS*) as well as positive regulators (*IRF4* and *IL2RG*), essential for effective immune responses. Consistent directional trends across datasets highlight the broader applicability of our screen results and uncover conserved regulatory programs that may inform gene-editing strategies for both NK and T cell therapies.

MED12 disruption augments NK cell antitumor potency

Prioritizing CRISPR screen hits, *MED12*, *ARIH2*, and *CCNC* emerged as top candidates for improving NK cell function. The Cdk8 kinase module (CKM) of the Mediator complex has emerged as a promising regulator of antitumor immunity.[22] Our screens demonstrate that *MED12* and *CCNC* similarly act as suppressors in NK cells (Figure 5A).

MED12 KO NK cells exhibited significantly enhanced cytotoxicity against resistant cancers (PATC148, MM1S, THP-1, and MOLM-14) in short-term and repeated tumor challenge assays (Figures 5B–5F and S7A–S7C). Deletion of *MED12* also enhanced the potency of IL-15-armored CAR-NK cells targeting human trophoblast cell surface glycoprotein antigen 2 (TROP2) and CD70 (Figures 5G, 5H, and S7D–S7F). Together, these findings establish *MED12* as a promising target to enhance CAR-NK cell antitumor potency.

ARIH2 and CCNC KO improves NK cell antitumor cytotoxicity by metabolic reprogramming

We next explored the effects of single and dual knockout of *CCNC* and *ARIH2* on NK cell function. CRISPR-edited NK cells displayed markedly improved killing of resistant targets, including PATC148 and Karpas-299 (T cell lymphoma) in both short-term and repeated challenge assays (Figures 6A–6C and S7G–S7K). IL-15-armored CAR-NK cells targeting TROP2 or CD70 similarly displayed enhanced cytotoxicity against multiple solid cancer models following single or dual knockout of *ARIH2* and *CCNC* (Figures 6D–6G and S7L–S7Q) including in 3D spheroids cultures. The improved antitumor potency correlated with enhanced metabolic fitness, evidenced by elevated basal, maximal and spare oxygen consumption rates, without impacting proliferation (Figures 6H–6K and S7R).

Mass cytometry (CyTOF) revealed contraction of inhibitory subsets (2, 4) and expansion of activated, proliferative clusters (2, 3, and 5) following *ARIH2* and *CCNC* deletion, both before and after tumor challenge. Interestingly, *ARIH2* deletion alone expanded inhibitory cluster 2, while co-deletion with *CCNC* reversed this effect (Figures 6L–6Q and S8A–S8C).

Target gene editing enhances CAR-NK cell potency *in vivo*

In an orthotopic murine pancreatic cancer model, *CCNC* KO, alone or with *ARIH2*, increased circulating CAR-NK cells and enhanced tumor infiltration suggesting improved migration (Figures 7A–7D). Tumor-infiltrating NK cells showed elevated granzyme B expression, with dual KO significantly reducing tumor burden (Figures 7C–7F). A second *in vivo* study using CD27CAR/IL-15 NK cells in a systemic myeloma model confirmed improved NK cell expansion and prolonged survival with *CCNC* or dual *ARIH2/CCNC* KO (Figures S9A–S9D). CRISPR gene-edited CAR-NK cells were well-tolerated, with no impact on body weight. Mass cytometry revealed expansion of activated cytotoxic clusters (4 and 5) and contraction of inhibitory populations (3) in both peritoneal fluid and spleen following dual KO (Figures 7G–7I and S9E–S9G).

Dual ARIH2 and CCNC KO enhances NK cell proliferation, activation, and inflammatory signaling

We next compared *ARIH2* and *CCNC* KO, two top hits from our screens, relative to *MED12* and the well-characterized checkpoint *CISH*. None of the edits affected viability or conferred cytokine-independent growth (Figures S10A and S10B). In rechallenge assays with PATC148, all KO conditions enhanced cytotoxicity, with *ARIH2/CCNC* DKO showing the strongest effect (Figure 8A). In an orthotopic pancreatic cancer mouse model, *ARIH2/CCNC* DKO or *CISH* KO TROP2CAR/IL-15-NK cells significantly reduced tumor burden and increased survival without toxicity (Figures 8B, 8C, S10C, and S10D).

To explore mechanisms behind the synergy, longitudinal CyTOF analyses revealed that *MED12, CCNC* and *CCNC/ARIH2* KO expanded clusters 7 and 8, characterized by expression of DNAM-1, CD69, NKG2D, CD25, Ki-67 and reduced quiescent cluster 1, indicating increased functional fitness under stress (Figures 8D–8F and S10E). Integrated surfaceome analysis from five CyTOF studies and seven CB-NK donors revealed

(E and F) Incucyte killing assay of *MED12*-ablated NK cells, repeatedly challenged with MM1S multiple myeloma cells (E) or MOLM-14 acute myeloid leukemia cells (F). Data depicted as mean normalized tumor growth ±SD (shaded in gray) ($n = 2$ CB donors; $^*p < 0.05$; unpaired t-test of the reciprocal of the scaled area under the tumor growth curve; AUC summary statistics shown in Figures S7B and S7C).
(G and H) Antigen-specific cytotoxicity of *MED12*-ablated CAR-NK cells targeting TROP2 and CD70, assessed by xCELLigence (PATC148; $n = 1$ donor) and Incucyte (THP-1; $n = 2$ donors) assays. Data depicted as mean normalized tumor growth ±SD (shaded in gray; $^*p < 0.05$; unpaired t-test of the reciprocal scaled area under the tumor growth curve; AUC and CAR constructs in Figures S7D–S7F). Also see Figure S7.

Please cite this article in press as: Biederstädt et al., Genome-wide CRISPR screens identify critical targets to enhance CAR-NK cell antitumor potency, Cancer Cell (2025), https://doi.org/10.1016/j.ccell.2025.07.021

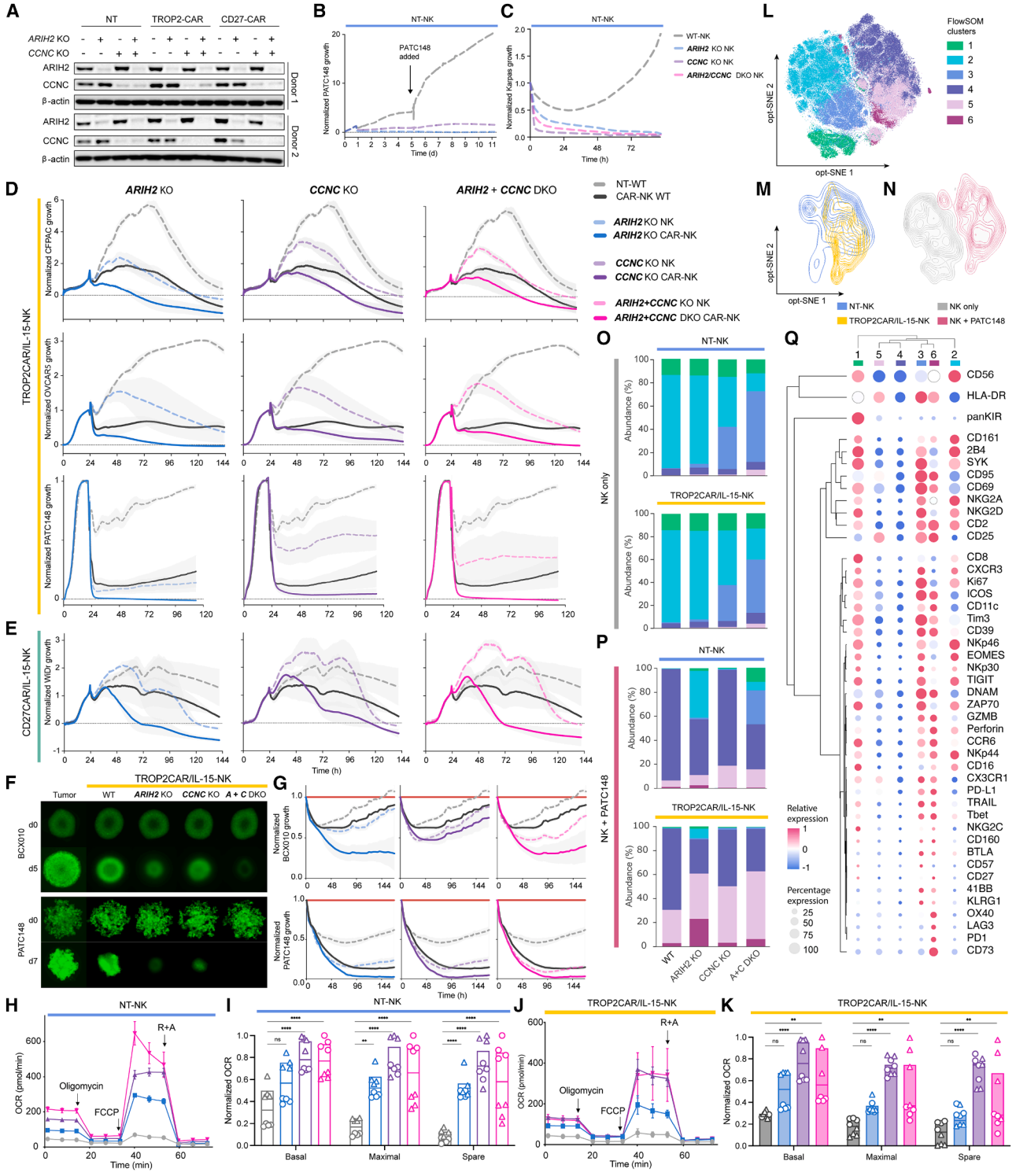

Figure 6. Multiplexed ARIH2/CCNC editing augments CAR-NK cell metabolic fitness and enhances tumor clearance

(A) Western blot analysis of ARIH2, CCNC, and beta-Actin in CRISPR-edited NT-NK and CAR-NK cells (TROP2CAR/IL-15 or CD27CAR/IL-15; *n* = 2 human CB donors; see also Figures S7G–S7I).

(B) *In vitro* PATC148 re-challenge assay of *ARIH2* and *CCNC*-deficient NK cells (xCELLigence; E:T = 4:1; *n* = 1 human CB donor; AUC shown in Figure S7J).

(C) *In vitro* tumor killing assay of *ARIH2* and *CCNC*-deficient NK cells co-cultured with Karpas-299 human T cell non-Hodgkin's lymphoma cells as assessed by Incucyte (E:T = 2:1; *n* = 1 human CB donor; AUC shown in Figure S7K).

(legend continued on next page)

Please cite this article in press as: Biederstädt et al., Genome-wide CRISPR screens identify critical targets to enhance CAR-NK cell antitumor potency, Cancer Cell (2025), https://doi.org/10.1016/j.ccell.2025.07.021

cooperative upregulation of activation markers in dual *CCNC*/*ARIH2* KO NK cells, which was particularly pronounced under *in vivo* TME pressure (Figures 8G and 8H). Cytokine profiling confirmed elevated pro-inflammatory and cytotoxic cytokines (Figure S11A).

Time-course expression analysis of *ARIH2*, *CCNC*, *MED12* and *CISH* in wild-type NK cells showed transient upregulation upon tumor challenge, followed by partial downregulation, indicating modest NK-intrinsic adaptive checkpoint regulation (Figure S12A). Single-cell RNA-seq revealed that *ARIH2* or *CCNC* KO induced proliferative, cytotoxic clusters (1 and 3) enriched for IFNγ, interleukin signaling, cell cycle, mTORC1, and DNA repair pathways, further amplified in dual KO NK cells. In contrast, *CISH* KO modestly expanded cluster 1, while *MED12* KO uniquely enriched cluster 2, marked by oxidative phosphorylation, fatty acid metabolism, and mTORC1 signaling (Figures 8I, 8J, and S12B–S12G).

Pathway analysis across 3,003 gene sets confirmed broad transcriptional reprogramming in *ARIH2*/*CCNC* and *MED12* KOs, with 21 enriched pathways largely exclusive to these groups (Figures 8K and S13). By contrast, *CISH*, *CCNC*, or ARIH2 KO alone altered only one or two pathways. Together, these results demonstrate that *ARIH2* and *CCNC* act cooperatively to reprogram NK cells into a metabolically fit, highly activated and cytokine responsive state under sustained tumor challenge.

DISCUSSION

Targeted gene editing has emerged as a powerful toolkit to enhance NK cell-based anticancer therapies.[10,11,34] However, designing more effective NK cell therapies requires deeper insights into the distinct cellular states driving therapeutic efficacy.[2] While recent single-cell multi-omics studies[31,44] and CRISPR screens in murine NK cells[45] have expanded our understanding, actionable genomic targets in primary human NK cells have remained largely unexplored. Bridging this gap, in this study we conducted a genome-wide CRISPR knockout screen in primary human NK cells under diverse clinically relevant experimental conditions. Using PreCiSE, we compiled a comprehensive atlas of NK cell regulators. Single cell transcriptomic data from patient-derived NK cells validated the clinical relevance of identified hits, offering insights into tumor-induced NK cell dysfunction.

The identified targets converged on critical transcriptional and post-translational regulatory complexes, such as the Mediator, CRL, and SAGA complexes, previously implicated in T cell biology,[22,46–49] highlighting shared pathways between NK and T cells. We validated *MED12, ARIH2*, and *CCNC* as previously unrecognized regulators of CAR-NK cell potency, underscoring their translational potential despite distinct NK and T cell biology.

Previous evidence implicates E3 ubiquitin ligases,[50] specifically the CRL complex,[47] as negative regulators of immune cell fitness. Our genome-wide screens identified five CRL members (*CISH, SOCS1, RNF7, CUL5*, and *ARIH2*) as critical NK cell regulators, highlighting the underappreciated role of post-translational modification (PTM) machinery in shaping NK cell functional states. These results position the CRL complex as a central hub of immune regulation and introduce PTM-targeting as a strategy in NK cell engineering.

Remarkably, our findings delineate *ARIH2* and *CCNC* as non-redundant regulators whose coordinated targeting substantially improves NK cell cytotoxicity and persistence, particularly evident under TME stress *in vivo*. Combined *ARIH2*/*CCNC* loss induced profound transcriptional reprogramming with enhancement of

(D) *In vitro* killing assays of *ARIH2*, *CCNC* and *ARIH2*/*CCNC* dual KO NK cells co-cultured with CFPAC human pancreatic cancer cells (E:T = 1:1), OVCAR5 human gastrointestinal cancer cells (E:T = 4:1) and PATC148 human pancreatic cancer cells (E:T = 4:1) as assessed by xCELLigence real-time cell analysis. Dashed lines indicate non-transduced NK cells; solid lines represent NK cells expressing a TROP2CAR/IL-15; color coding denotes CRISPR perturbations versus wildtype (WT) controls. Data represented as mean ± SEM (SEM shaded in light gray) for $n = 2$ human NK cell donors (CFPAC, OVCAR5, WiDr) and $n = 3$ (PATC148); AUC summary statistics shown in Figure S7N).

(E) *In vitro* killing assays of *ARIH2*, *CCNC* and *ARIH2*/*CCNC* dual KO NK cells co-cultured with WiDr human colorectal cancer cells (E:T = 1:1) as assessed by xCELLigence real-time cell analysis. Dashed lines indicate non-transduced NK cells; solid lines represent NK cells expressing a CD70-directed natural ligand CD27 CAR molecule with IL-15 armoring; color coding denotes CRISPR perturbations versus wildtype (WT) controls. ($n = 2$ human CB donors; data represented as mean ± SEM (shaded in light gray); AUC summary statistics shown in Figure S7N, right).

(F and G) Representative images (F) and killing kinetics (G) of 3D spheroid killing assays of CRISPR-perturbed TROP2CAR/IL-15-NK cells co-cultured with BCX010 and PATC148 cancer spheroids as assessed by Incucyte live cell imaging. Effector-to-target (E:T) ratios were 3:1 (BCX010) and 1.25:1 (PATC148); data presented as mean normalized tumor growth ±SEM (tumor only, red; WT, gray; *ARIH2* KO, blue; *CCNC* KO purple; *ARIH2*/*CCNC* DKO, pink; NT-NK conditions, dashed lines; CAR-NK conditions, solid lines; SEM shaded in light gray) (G); $n = 3$ human NK cell donors (see also Figure S7Q).

(H and J) Representative oxygen consumption rate (OCR) trace of *ARIH2*, *CCNC* and *ARIH2*/*CCNC* KO NT-NK (H) and TROP2CAR/IL-15-NK cells (J) under resting and challenge conditions as assessed by Seahorse analysis. Addition of oligomycin, carbonyl cyanide-4 (trifluoromethoxy) phenylhydrazone (FCCP) and rotenone + antimycin A (R + A) is indicated by arrows ($n = 2$ human NK cell donors in 4 replicates; mean ± SD; OCR traces are representative results from two independent human NK cell donors).

(I and K) Basal, maximum and spare normalized oxygen consumption rate (OCR) of *ARIH2*, *CCNC* and *ARIH2*/*CCNC* KO NT-NK (I) and TROP2CAR/IL-15-NK cells (K) ($n = 2$ donors; 4 technical replicates; symbol shapes indicate independent biological NK cell donors; normalized to maximum metabolic rate). Data represented as box-and-whiskers plot; box limits represent quartiles, whiskers indicate minimum and maximum values, the horizontal solid line represents the median OCR. (Two-way ANOVA corrected for multiple comparisons by Tukey test; ns, not significant; $^{**}p < 0.01$, $^{****}p < 0.0001$).

(L–N) High-dimensional phenotypic characterization of CRISPR-edited NK cells as assessed by mass cytometry, see also Figure S8A. (L) Opt-SNE map of CRISPR-perturbed primary human NK cells before and after PATC148 tumor co-culture, overlayed with FlowSOM clusters. (M and N) Contour plots indicating single cell projections for NT-NK vs. TROP2CAR/IL-15-NK cells (M) before or after challenge with PATC148 pancreatic cancer cells (N).

(O and P) Bar charts depicting FlowSOM cluster composition in primary human NT-NK and TROP2CAR/IL-15-NK cells upon ablation of *ARIH2*, *CCNC* and *ARIH2*/*CCNC* before (O) and after (P) PATC148 challenge (FlowSOM clusters: (1) green, (2) cyan, (3) light blue, (4) purple, (5) rose, (6) magenta; see also Figures S8B and S8C).

(Q) Heatmap indicating z-transformed median expression per channel and percentage marker expression of gene-edited NK cells across FlowSOM clusters. Also see Figures S7 and S8.

Please cite this article in press as: Biederstädt et al., Genome-wide CRISPR screens identify critical targets to enhance CAR-NK cell antitumor potency, Cancer Cell (2025), https://doi.org/10.1016/j.ccell.2025.07.021

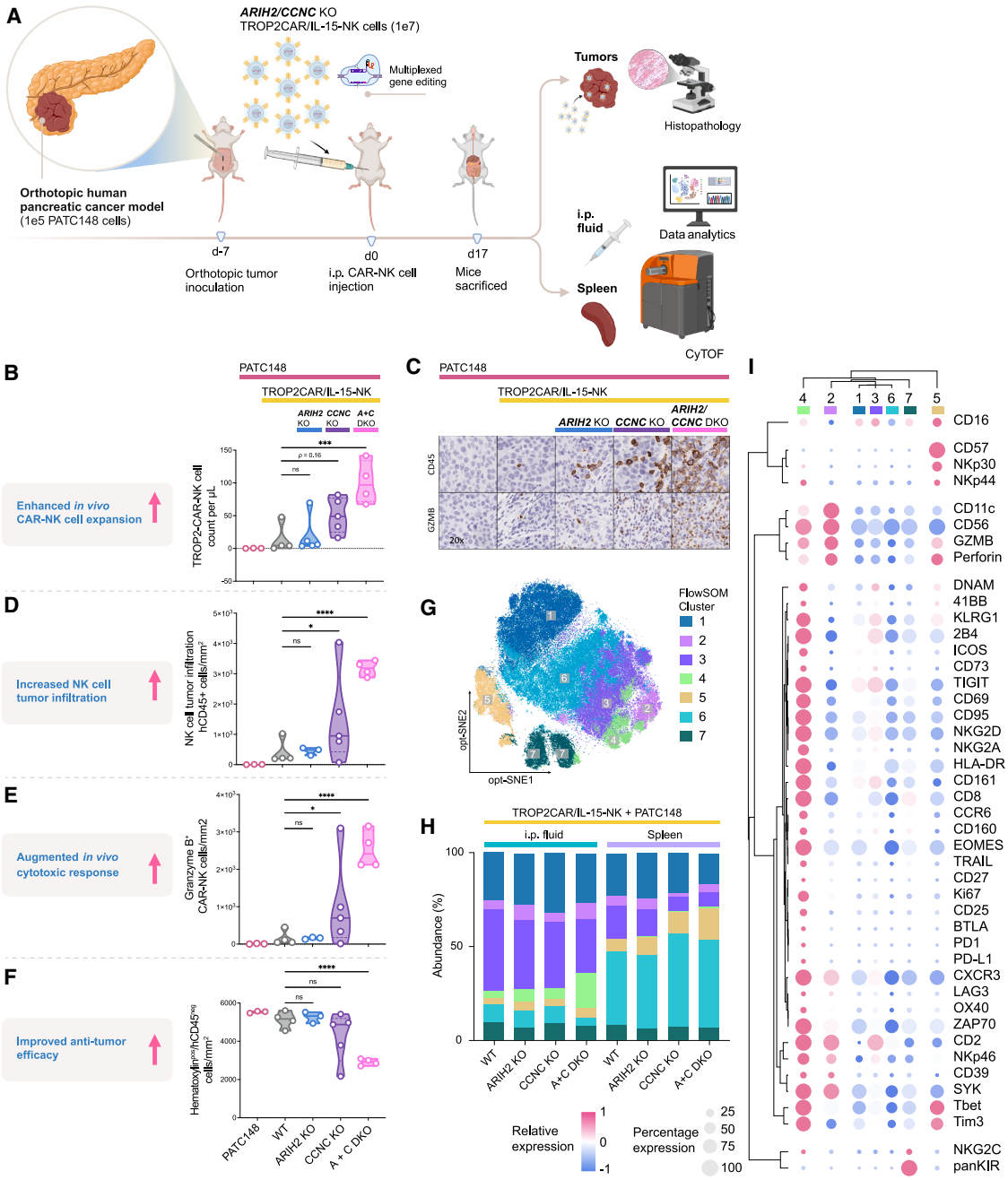

Figure 7. Multiplexed CRISPR editing boosts CAR-NK cell potency *in vivo*

(A) Schematic depicting an *in vivo* study assessing antitumor efficacy of *ARIH2* KO, *CCNC* KO and *ARIH2*/*CCNC* DKO TROP2CAR/IL-15-NK cells in an orthotopic pancreatic cancer mouse model (n = 5 NSG mice per condition; see also Figures S9A–S9D).

(B) Flow cytometry-based analysis of CRISPR-edited TROP2CAR/IL-15-NK cells circulating in the peripheral blood on d10 post injection. Data represented as truncated violin plots (bold line represents median, dashed lines represents interquartile range; symbols represent number of mice per group; plots truncated at minimum and maximum values); one-way ANOVA; ns, not significant; ***$p < 0.001$.

(C–F) Immunohistochemical (IHC) analysis of NK cell tumor infiltration (C and D), assessed by hCD45 positive cells, intratumoral Granzyme B staining (C and E) and assessment of hematoxylin positive, hCD45 negative tumor cells (F); data represented as truncated violin plots (bold line, median; dashed lines, interquartile range; symbols, number of mice per group; plots truncated at minimum and maximum values); one-way ANOVA; ns, not significant; *$p < 0.05$, ****$p < 0.0001$. (C) Representative IHC image of an orthotopic tumor specimen stained for hCD45 (top) and Granzyme B (bottom).

(G) Mass cytometry-enabled phenotypic profiling of gene-edited NK cells represented as Opt-SNE map overlaid with FlowSOM metaclusters (See also Figures S9E–S9G).

(legend continued on next page)

Please cite this article in press as: Biederstädt et al., Genome-wide CRISPR screens identify critical targets to enhance CAR-NK cell antitumor potency, Cancer Cell (2025), https://doi.org/10.1016/j.ccell.2025.07.021

IFNγ signaling, interleukin responsiveness, mTORC1 activation, cell cycle progression, and DNA repair pathways, surpassing the impact of single-gene disruptions. These data highlight the complementary roles of *ARIH2* and *CCNC* in orchestrating NK cell effector functions, making them compelling targets for further clinical development. These findings support multiplexed engineering of transcriptional, post-translational, and metabolic programs to overcome resistance and boost NK potency. As multiplex gene-editing technologies advance, rational combination of such targets offers a promising strategy to overcome resistance in solid tumors, where current cell therapies show limited efficacy. Central to this resistance is the immunosuppressive TME, which imposes unique barriers to NK cell function. Previously, we showed *TGFBR2* KO improves NK cell responses to glioblastoma and AML.[12,51] Our screens further support roles for *SMAD2* and *SMAD4* in TGF-β1-mediated NK cell immunosuppression, with *SMAD* deletion enhancing NK antitumor potency.[52–54]

We also identified targets within the HIF1α pathway suitable for engineering hypoxia-resistant NK cells.[55,56] While core components such as *HIF1A*, *HIF1B*, or their upstream regulators were not recovered, likely due to biological redundancy or sgRNA inefficiency, several transcriptional HIF1α targets emerged as functional regulators, pointing to opportunities for selectively rewiring hypoxia adaptation without inducing broad pleiotropic effects.

Intriguingly, our genome-wide screens also identified several tumor suppressors (*PTEN* and TP53 regulators) as actionable NK cell targets. These findings reinforce an emerging paradigm in immune cell engineering wherein therapeutic cells may exploit oncogenic pathways to improve metabolic fitness under nutrient stress,[19,25,32,57] as observed with MYC and mTOR upregulation following *CISH* KO in NK cells.[10,11,58,59]

Our study was unable to detect genes with functional paralogs, highlighting the need for combinatorial screens to uncover epistatic interactions. Second, epigenetic NK cell regulation governing transcriptional activation remained unexplored and warrants future studies using non-heritable CRISPR editors. Finally, synthetic gene programs, not physiologically expressed by NK cells, were not assessed in our platform and will require pooled knockin strategies.

Nonetheless, we identified several positive regulators of NK cell function including genes involved in immune response (*IRF4*, *TRAF1*), cell cycle control (*CDK6* and *PPP6C*), mitochondrial respiration (*FDX1L*), metabolic regulation (*LIPT2, DOLK, MOGS, PPCDC, SEPHS2)*, chromatin accessibility (*CHRAC*) and DNA repair (*POLE*) which may drive heightened NK cell function when transcriptionally induced. Our TF library screens further identified *BATF3*, *IRF4*, *TFAP4*, and *JUNB*, transcription factors previously implicated in enhancing effector function and preventing exhaustion in CAR-T cells.[25,26,60] Notably, *BATF3 and TFAP4*, also ranked among top hits in recent pooled knockin screens, where they conferred metabolic and functional advantages in CAR-T cells.[60] These results suggest that ectopic overexpression of select transcriptional regulators, including through site-directed homology-directed repair (HDR) could enhance NK cell function.[61,62]

Advances in CRISPR enzyme design and delivery, including high-fidelity nucleases, AI-optimized guide design, and non-viral delivery systems, promise to improve the specificity, safety and scalability of immune cell editing for clinical translation.[63–66] Our study highlights the power of CRISPR-based discovery platforms to uncover cooperative gene networks that govern NK cell function and to guide the rational design of next-generation NK cell therapies for patients with otherwise treatment-refractory cancers.

RESOURCE AVAILABILITY

Lead contact

Further information and requests for resources and reagents should be directed to and will be fulfilled by Katayoun Rezvani (krezvani@mdanderson.org).

Materials availability

CRISPR sgRNA transfer plasmid generated in this study is available from the lead contact upon request.

Data and code availability

- Original western blot images and NK cell scRNA-seq data generated in this study were deposited to Zenodo and are publicly available as of the date of publication.
- Microscopy data and raw sequencing files of NK scRNA-seq and CRISPR screen sgRNA sequencing will be shared by the lead contact upon request.
- No custom code was used for the generation of the manuscript.
- Any additional information required to reanalyze the data reported in this paper is available from the lead contact upon request.

ACKNOWLEDGMENTS

This work was supported in part by the generous philanthropic contributions to The University of Texas MD Anderson Cancer Center Institute for Cell Therapy Discovery and Innovation, including lead commitments from Meg and Kirk Gentle, Lindonlight Collective, The Marcus Foundation, Inc., The Margery L. Block Foundation, Melville Foundation and Tanoto Foundation and additional significant support from The James B. and Lois R. Archer Charitable Foundation, Ann and Clarence Cazalot, The Cockrell Foundation, The Cyvia & Melvyn Wolff Family Foundation; Vijay and Marie Goradia, Melvyn N. Klein, Marek Family Foundation, Gayle Stoffel, The McCombs Foundation, The Walters Family, and MD Anderson's Accelerator Fund; The Sally Cooper Murray endowment; by grants (grant nos. 1 R01 CA211044-01, 5 P01CA148600-03, 1 R01CA280827-01, and 1 R01CA288617-01) from the National Institutes of Health (NIH); by the Specialized Program of Research Excellence (SPORE) grants in Ovarian Cancer (5P50CA281701-02) and Brain Cancer (P50CA127001).

The MD Anderson Cancer Center Advanced Technology Genomics Core (ATGC) Facility was supported in part by a grant from the NIH (grant nos. CA016672, 1S10OD024977-01). The Flow Cytometry and Cellular Imaging Core Facility was supported in part by The University of Texas MD Anderson Cancer Center, P30CA016672, a Shared Instrumentation Award from the Cancer Prevention Research Institution of Texas (CPRIT). X.R.J. and Y.L. are

(H) Bar chart depicting the alterations in FlowSOM cluster composition induced by targeted *ARIH2*, *CCNC* and *ARIH2/CCNC* editing in TROP2CAR/IL-15-NK cells derived from i.p. fluid and spleens from an orthotopic murine model of human pancreatic cancer (FlowSOM clusters: (1) dark blue, (2) violet, (3) purple, (4) light green, (5) beige, (6) cyan, (7) dark green; see also Figures S9E–S9G).
(I) Heatmap depicting the relative and percentage marker expression per FlowSOM metacluster. Color indicates z score-normalized median expression per channel, circle size indicates percentage expression. Also see Figure S9.

Please cite this article in press as: Biederstädt et al., Genome-wide CRISPR screens identify critical targets to enhance CAR-NK cell antitumor potency, Cancer Cell (2025), https://doi.org/10.1016/j.ccell.2025.07.021

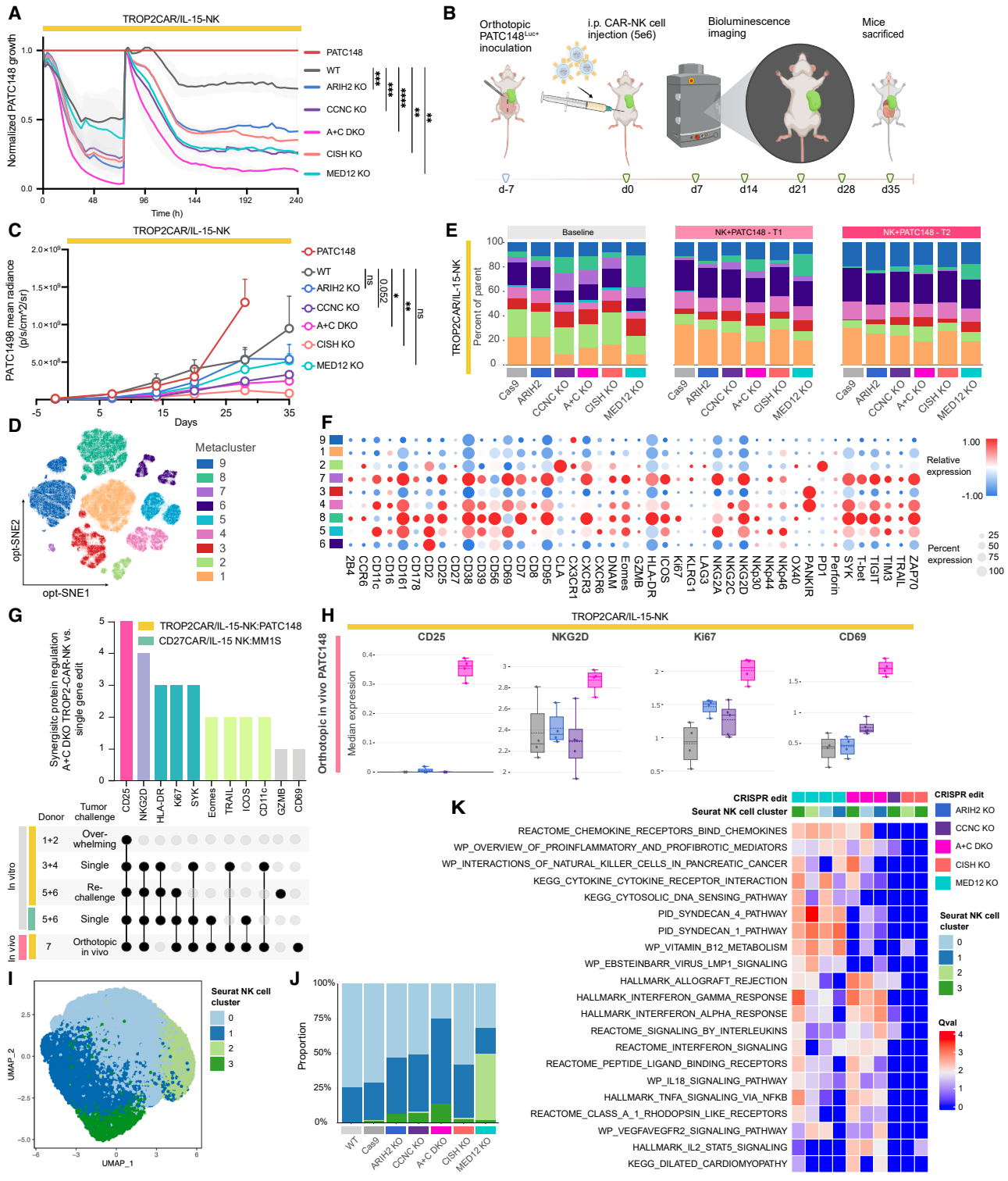

Figure 8. *ARIH2* and *CCNC* KO synergize to augment NK cell proliferation, activation, interleukin signaling and interferon gamma response

(A) *In vitro* tumor re-challenge assay of CRISPR-edited NK cells deficient for *ARIH2*, *CCNC*, *ARIH2*/*CCNC*, *CISH*, or *MED12*, co-cultured with PATC148 human pancreatic cancer cells as assessed by xCELLigence real-time cell analysis. Data represented as mean ± SEM (shaded in light gray); NK cell killing normalized to timepoint 0 and tumor. (E:T = 6:1; $n = 2$ human NK cell donors; one-way ANOVA for area under the PATC148 growth curve; $^{**}p < 0.01$, $^{***}p < 0.001$, $^{****}p < 0.0001$) (See also Figures S10A and S10B).

(B and C) Conceptual depicting the orthotopic pancreatic cancer mouse model to assess the *in vivo* antitumor efficacy of CRISPR-engineered TROP2CAR/IL-15-NK cells.

(legend continued on next page)

supported by CPRIT Research Training Award RP210028. Figures were generated using Adobe Illustrator and BioRender.

AUTHOR CONTRIBUTIONS

A.B., R.B., and K.R. conceptualized the study. A.B., R.B., J.-M.P., N.U., R.S., and F.R.C., May Daher, J.W., B.L., P.B., S.I., S.A., Ping Li, V.W., I.B., M.S., J.J., B.K., X.R.J., A.K.N.C., S.R., and Y.L. performed experiments and interpreted and analyzed data. A.B., Merve Dede, J.-M.P., H.F., and D.X. performed bioinformatics analysis. N.W.F. performed pathology analysis on mice samples. R.B., J.-M.P., N.U., R.S., B.L., J.W., S.A., May Daher, Merve Dede, B.L., D. X., P.B., Y.L., H.R., P.L., P.Z., S.T., E.L., E.J.S., L.M.-F., G.M.D., and K.C. provided advice on experiments, reviewed manuscript, and provided comments. A.B. drafted the original manuscript, which was reviewed and edited by L. M.-F., G.M.D., and K.R.

DECLARATION OF INTERESTS

R.B., N.U., May Daher., H.R., P.B., S.A., M.S., Paul Lin., Y.L., E.L., E.J.S., K.R., and The University of Texas MD Anderson Cancer Center have an institutional financial conflict of interest with Takeda Pharmaceuticals. R.B., S.A., E.L., E.J. S., K.R. and The University of Texas MD Anderson Cancer Center have an institutional financial conflict of interest with Affimed. K.R. participates on the Scientific Advisory Board for Avenge Bio, Virogin Biotech, Navan Technologies, Caribou Biosciences, Bit Bio Limited, Replay Holdings, oNKo Innate, The Alliance for Cancer Gene Therapy ACGT, Innate Pharma and Shinobi Therapeutics. K.R. is the scientific founder of Syena. May Daher participates on the Scientific Advisory Board of Cellsbin. E.J.S. participates on the Scientific Advisory Board for Adaptimmune Limited, Axio Research, Celaid Therapeutics, FibroBiologics, Navan Technologies, New York Blood Center, and Zelluna Immunotherapy. The remaining authors declare no competing interests.

STAR★METHODS

Detailed methods are provided in the online version of this paper and include the following:

SUPPLEMENTAL INFORMATION

Supplemental information can be found online at https://doi.org/10.1016/j.ccell.2025.07.021.

Received: December 2, 2024
Revised: May 30, 2025
Accepted: July 21, 2025

REFERENCES

1. Liu, E., Marin, D., Banerjee, P., Macapinlac, H.A., Thompson, P., Basar, R., Nassif Kerbauy, L., Overman, B., Thall, P., Kaplan, M., et al. (2020). Use of

(D) PATC148 tumor growth (mean bioluminescent radiance) in orthotopic pancreatic cancer-bearing mice infused with *ARIH2* KO, *CCNC* KO, *ARIH2*/*CCNC* DKO, *CISH* KO or *MED12* KO TROP2CAR/IL-15-NK cells ($n = 4$ per condition; one-way ANOVA for day 35 mean radiance (ns, not significant, $^{*}p < 0.05$, $^{**}p < 0.01$). (See also Figures S10C and S10D).
(D–F) Deep phenotypic profiling of gene-edited TROP2CAR/IL-15-NK cells by mass cytometry. (D) Opt-SNE projection of CRISPR-edited NK cells at baseline and after one and two PATC148 tumor challenges, overlayed with FlowSOM metaclusters. (E) Bar charts depicting dynamic regulation of NK cells clusters in CRISPR-edited TROP2CAR/IL-15-NK cells at baseline (left) and after one (middle) and two (right) challenges with PATC148 pancreatic cancer cells. (F) Heatmap depicting z-transformed median expression per channel and percentage surface marker expression of CRISPR-perturbed NK cells across FlowSOM metaclusters.
(G) UpSet plot showing the number of independent experiments, demonstrating cooperative protein induction for NK cell activating markers in *ARIH2*/*CCNC* DKO CAR-NK cells compared to expected additive effects from *ARIH2* or *CCNC* single KOs (pseudo-Loewe sum analysis; $n = 7$ CB donors).
(H) Bar charts depicting median expression of CD25, NKG2D, Ki67 and CD69 by infused CRISPR-KO TROP2CAR/IL-15-NK cells harvested from the i.p. fluid of tumor-bearing (PATC148) mice, as assessed by mass cytometry ($n = 4$ per condition; gray, WT control; blue, *ARIH2* KO; purple, *CCNC* KO; pink, *ARIH2*/*CCNC* DKO).
(I–K) scRNA-seq studies of CRISPR-edited NK cells deficient for *ARIH2*, *CCNC*, *ARIH2*/*CCNC*, *CISH*, or *MED12*, co-cultured with PATC148 cells. (I) UMAP projection of gene-edited NK cells, overlayed with Seurat clusters. (J) Bar charts depicting Seurat NK cell cluster composition in CRISPR-edited TROP2CAR/IL-15-NK cells after tumor challenge. (K) Heatmap depicting significantly enriched pathways in CRISPR-edited CAR-NK cells compared to non-edited controls. Top annotation bars indicate experimental conditions and corresponding Seurat-defined NK cell clusters. Also see Figure S10.

CAR-Transduced Natural Killer Cells in CD19-Positive Lymphoid Tumors. N. Engl. J. Med. *382*, 545–553. https://doi.org/10.1056/NEJMoa1910607.

2. Marin, D., Li, Y., Basar, R., Rafei, H., Daher, M., Dou, J., Mohanty, V., Dede, M., Nieto, Y., Uprety, N., et al. (2024). Safety, efficacy and determinants of response of allogeneic CD19-specific CAR-NK cells in CD19(+) B cell tumors: a phase 1/2 trial. Nat. Med. *30*, 772–784. https://doi.org/10.1038/s41591-023-02785-8.

3. Liu, E., Tong, Y., Dotti, G., Shaim, H., Savoldo, B., Mukherjee, M., Orange, J., Wan, X., Lu, X., Reynolds, A., et al. (2018). Cord blood NK cells engineered to express IL-15 and a CD19-targeted CAR show long-term persistence and potent antitumor activity. Leukemia *32*, 520–531. https://doi.org/10.1038/leu.2017.226.

4. Li, Y., Hermanson, D.L., Moriarity, B.S., and Kaufman, D.S. (2018). Human iPSC-Derived Natural Killer Cells Engineered with Chimeric Antigen Receptors Enhance Anti-tumor Activity. Cell Stem Cell *23*, 181–192.e5. https://doi.org/10.1016/j.stem.2018.06.002.

5. Li, L., Mohanty, V., Dou, J., Huang, Y., Banerjee, P.P., Miao, Q., Lohr, J.G., Vijaykumar, T., Frede, J., Knoechel, B., et al. (2023). Loss of metabolic fitness drives tumor resistance after CAR-NK cell therapy and can be overcome by cytokine engineering. Sci. Adv. *9*, eadd6997. https://doi.org/10.1126/sciadv.add6997.

6. Zhang, Q., Bi, J., Zheng, X., Chen, Y., Wang, H., Wu, W., Wang, Z., Wu, Q., Peng, H., Wei, H., et al. (2018). Blockade of the checkpoint receptor TIGIT prevents NK cell exhaustion and elicits potent anti-tumor immunity. Nat. Immunol. *19*, 723–732. https://doi.org/10.1038/s41590-018-0132-0.

7. Gallois, A., Silva, I., Osman, I., and Bhardwaj, N. (2014). Reversal of natural killer cell exhaustion by TIM-3 blockade. OncoImmunology *3*, e946365. https://doi.org/10.4161/21624011.2014.946365.

8. André, P., Denis, C., Soulas, C., Bourbon-Caillet, C., Lopez, J., Arnoux, T., Bléry, M., Bonnafous, C., Gauthier, L., Morel, A., et al. (2018). Anti-NKG2A mAb Is a Checkpoint Inhibitor that Promotes Anti-tumor Immunity by Unleashing Both T and NK Cells. Cell *175*, 1731–1743.e13. https://doi.org/10.1016/j.cell.2018.10.014.

9. Peng, L., Renauer, P.A., Sferruzza, G., Yang, L., Zou, Y., Fang, Z., Park, J. J., Chow, R.D., Zhang, Y., Lin, Q., et al. (2025). In vivo AAV–SB-CRISPR screens of tumor-infiltrating primary NK cells identify genetic checkpoints of CAR-NK therapy. Nat. Biotechnol. *43*, 752–761. https://doi.org/10.1038/s41587-024-02282-4.

10. Zhu, H., Blum, R.H., Bernareggi, D., Ask, E.H., Wu, Z., Hoel, H.J., Meng, Z., Wu, C., Guan, K.L., Malmberg, K.J., and Kaufman, D.S. (2020). Metabolic Reprograming via Deletion of CISH in Human iPSC-Derived NK Cells Promotes In Vivo Persistence and Enhances Anti-tumor Activity. Cell Stem Cell *27*, 224–237.e6. https://doi.org/10.1016/j.stem.2020.05.008.

11. Daher, M., Basar, R., Gokdemir, E., Baran, N., Uprety, N., Nunez Cortes, A. K., Mendt, M., Kerbauy, L.N., Banerjee, P.P., Shanley, M., et al. (2021). Targeting a cytokine checkpoint enhances the fitness of armored cord blood CAR-NK cells. Blood *137*, 624–636. https://doi.org/10.1182/blood.2020007748.

12. Shaim, H., Shanley, M., Basar, R., Daher, M., Gumin, J., Zamler, D.B., Uprety, N., Wang, F., Huang, Y., Gabrusiewicz, K., et al. (2021). Targeting the αv integrin/TGF-β axis improves natural killer cell function against glioblastoma stem cells. J. Clin. Investig. *131*, e142116. https://doi.org/10.1172/jci142116.

13. Guo, X., Mahlakõiv, T., Ye, Q., Somanchi, S., He, S., Rana, H., DiFiglia, A., Gleason, J., van der Touw, W., Hariri, R., and Zhang, X. (2021). *CBLB* ablation with CRISPR/Cas9 enhances cytotoxicity of human placental stem cell-derived NK cells for cancer immunotherapy. J. Immunother. Cancer *9*, e001975. https://doi.org/10.1136/jitc-2020-001975.

14. Mohammadian Gol, T., Kim, M., Sinn, R., Ureña-Bailén, G., Stegmeyer, S., Gratz, P.G., Zahedipour, F., Roig-Merino, A., Antony, J.S., and Mezger, M. (2023). CRISPR-Cas9-Based Gene Knockout of Immune Checkpoints in Expanded NK Cells. Int. J. Mol. Sci. *24*, 16065.

15. Yamamoto, K., Blum, R., and Kaufman, D.S. (2020). ADAM17-Deficient Pluripotent Stem Cell-Derived Natural Killer Cells Possess Improved Antibody-Dependent Cellular Cytotoxicity and Antitumor Activity. Blood *136*, 2. https://doi.org/10.1182/blood-2020-137766.

16. Pomeroy, E.J., Hunzeker, J.T., Kluesner, M.G., Lahr, W.S., Smeester, B. A., Crosby, M.R., Lonetree, C.L., Yamamoto, K., Bendzick, L., Miller, J. S., et al. (2020). A Genetically Engineered Primary Human Natural Killer Cell Platform for Cancer Immunotherapy. Mol. Ther. *28*, 52–63. https://doi.org/10.1016/j.ymthe.2019.10.009.

17. Naeimi Kararoudi, M., Elmas, E., Lamb, M., Chakravarti, N., Trikha, P., and Lee, D.A. (2018). Disruption of SOCS3 Promotes the Anti-Cancer Efficacy of Primary NK Cells. Blood *132*, 5687. https://doi.org/10.1182/blood-2018-99-116621.

18. Berrien-Elliott, M.M., Pamela, W., Neal, C., Wagner, J.A., Becker-Hapak, M., Schappe, T., Cooper, M.L., Mace, E.M., and Fehniger, T.A. (2019). Primary Human NK Cell Gene-Editing Reveals a Critical Role for NKG2A in Cytokine-Induced Memory-like NK Cell Responses. Blood *134*, 3237. https://doi.org/10.1182/blood-2019-129162.

19. Carnevale, J., Shifrut, E., Kale, N., Nyberg, W.A., Blaeschke, F., Chen, Y. Y., Li, Z., Bapat, S.P., Diolaiti, M.E., O'Leary, P., et al. (2022). RASA2 ablation in T cells boosts antigen sensitivity and long-term function. Nature *609*, 174–182. https://doi.org/10.1038/s41586-022-05126-w.

20. Shifrut, E., Carnevale, J., Tobin, V., Roth, T.L., Woo, J.M., Bui, C.T., Li, P. J., Diolaiti, M.E., Ashworth, A., and Marson, A. (2018). Genome-wide CRISPR Screens in Primary Human T Cells Reveal Key Regulators of Immune Function. Cell *175*, 1958–1971.e15. https://doi.org/10.1016/j.cell.2018.10.024.

21. Wang, D., Prager, B.C., Gimple, R.C., Aguilar, B., Alizadeh, D., Tang, H., Lv, D., Starr, R., Brito, A., Wu, Q., et al. (2021). CRISPR Screening of CAR T Cells and Cancer Stem Cells Reveals Critical Dependencies for Cell-Based Therapies. Cancer Discov. *11*, 1192–1211. https://doi.org/10.1158/2159-8290.CD-20-1243.

22. Freitas, K.A., Belk, J.A., Sotillo, E., Quinn, P.J., Ramello, M.C., Malipatlolla, M., Daniel, B., Sandor, K., Klysz, D., Bjelajac, J., et al. (2022). Enhanced T cell effector activity by targeting the Mediator kinase module. Science *378*, eabn5647. https://doi.org/10.1126/science.abn5647.

23. Shah, N., Martin-Antonio, B., Yang, H., Ku, S., Lee, D.A., Cooper, L.J.N., Decker, W.K., Li, S., Robinson, S.N., Sekine, T., et al. (2013). Antigen presenting cell-mediated expansion of human umbilical cord blood yields log-scale expansion of natural killer cells with anti-myeloma activity. PLoS One *8*, e76781. https://doi.org/10.1371/journal.pone.0076781.

24. Schmidt, R., Steinhart, Z., Layeghi, M., Freimer, J.W., Bueno, R., Nguyen, V.Q., Blaeschke, F., Ye, C.J., and Marson, A. (2022). CRISPR activation and interference screens decode stimulation responses in primary human T cells. Science *375*, eabj4008. https://doi.org/10.1126/science.abj4008.

25. Lynn, R.C., Weber, E.W., Sotillo, E., Gennert, D., Xu, P., Good, Z., Anbunathan, H., Lattin, J., Jones, R., Tieu, V., et al. (2019). c-Jun overexpression in CAR T cells induces exhaustion resistance. Nature *576*, 293–300. https://doi.org/10.1038/s41586-019-1805-z.

26. Seo, H., González-Avalos, E., Zhang, W., Ramchandani, P., Yang, C., Lio, C.-W.J., Rao, A., and Hogan, P.G. (2021). BATF and IRF4 cooperate to counter exhaustion in tumor-infiltrating CAR T cells. Nat. Immunol. *22*, 983–995. https://doi.org/10.1038/s41590-021-00964-8.

27. Küçük, C., Iqbal, J., Hu, X., Gaulard, P., De Leval, L., Srivastava, G., Au, W. Y., McKeithan, T.W., and Chan, W.C. (2011). *PRDM1* is a tumor suppressor gene in natural killer cell malignancies. Proc. Natl. Acad. Sci. USA *108*, 20119–20124. https://doi.org/10.1073/pnas.1115128108.

28. Smith, M.A., Maurin, M., Cho, H.I., Becknell, B., Freud, A.G., Yu, J., Wei, S., Djeu, J., Celis, E., Caligiuri, M.A., and Wright, K.L. (2010). PRDM1/Blimp-1 controls effector cytokine production in human NK cells. J. Immunol. *185*, 6058–6067. https://doi.org/10.4049/jimmunol.1001682.

29. Selvarajan, V., Osato, M., Nah, G.S.S., Yan, J., Chung, T.H., Voon, D.C.C., Ito, Y., Ham, M.F., Salto-Tellez, M., Shimizu, N., et al. (2017). RUNX3 is oncogenic in natural killer/T-cell lymphoma and is transcriptionally regulated by MYC. Leukemia *31*, 2219–2227. https://doi.org/10.1038/leu.2017.40.

30. Levanon, D., Negreanu, V., Lotem, J., Bone, K.R., Brenner, O., Leshkowitz, D., and Groner, Y. (2014). Transcription factor Runx3 regulates interleukin-15-dependent natural killer cell activation. Mol. Cell Biol. *34*, 1158–1169. https://doi.org/10.1128/mcb.01202-13.

31. Tang, F., Li, J., Qi, L., Liu, D., Bo, Y., Qin, S., Miao, Y., Yu, K., Hou, W., Li, J., et al. (2023). A pan-cancer single-cell panorama of human natural killer cells. Cell *186*, 4235–4251.e20. https://doi.org/10.1016/j.cell.2023.07.034.

32. Briercheck, E.L., Trotta, R., Chen, L., Hartlage, A.S., Cole, J.P., Cole, T.D., Mao, C., Banerjee, P.P., Hsu, H.T., Mace, E.M., et al. (2015). PTEN is a negative regulator of NK cell cytolytic function. J. Immunol. *194*, 1832–1840. https://doi.org/10.4049/jimmunol.1401224.

33. Crinier, A., Dumas, P.Y., Escalière, B., Piperoglou, C., Gil, L., Villacreces, A., Vély, F., Ivanovic, Z., Milpied, P., Narni-Mancinelli, É., and Vivier, É. (2021). Single-cell profiling reveals the trajectories of natural killer cell differentiation in bone marrow and a stress signature induced by acute myeloid leukemia. Cell. Mol. Immunol. *18*, 1290–1304. https://doi.org/10.1038/s41423-020-00574-8.

34. Delconte, R.B., Kolesnik, T.B., Dagley, L.F., Rautela, J., Shi, W., Putz, E.M., Stannard, K., Zhang, J.-G., Teh, C., Firth, M., et al. (2016). CIS is a potent checkpoint in NK cell–mediated tumor immunity. Nat. Immunol. *17*, 816–824. https://doi.org/10.1038/ni.3470.

35. Chen, H., He, B., Zhong, S., Huang, D., Deng, S., Liu, Q., Li, C., Huang, L., and Xu, N. (2023). Disruption of SOCS1 Promotes the Antitumor Activity of CD19-Specific CAR NK Cells Coexpressing IL-15. Blood *142*, 6829. https://doi.org/10.1182/blood-2023-182516.

36. Kim, W.S., Kim, M.J., Kim, D.O., Byun, J.-E., Huy, H., Song, H.Y., Park, Y.-J., Kim, T.-D., Yoon, S.R., Choi, E.-J., et al. (2017). Suppressor of Cytokine Signaling 2 Negatively Regulates NK Cell Differentiation by Inhibiting JAK2 Activity. Sci. Rep. *7*, 46153. https://doi.org/10.1038/srep46153.

37. Lee, S.H., Yun, S., Piao, Z.H., Jeong, M., Kim, D.O., Jung, H., Lee, J., Kim, M.J., Kim, M.S., Chung, J.W., et al. (2010). Suppressor of cytokine signaling 2 regulates IL-15-primed human NK cell function via control of phosphorylated Pyk2. J. Immunol. *185*, 917–928. https://doi.org/10.4049/jimmunol.1000784.

38. Bista, P., Zeng, W., Ryan, S., Bailly, V., Browning, J.L., and Lukashev, M.E. (2010). TRAF3 controls activation of the canonical and alternative NFkappaB by the lymphotoxin beta receptor. J. Biol. Chem. *285*, 12971–12978. https://doi.org/10.1074/jbc.M109.076091.

39. Rafei, H., Basar, R., Acharya, S., Hsu, Y.-S., Liu, P., Zhang, D., Bohn, T., Liang, Q., Mohanty, V., Upadhyay, R., et al. (2025). CREM is a regulatory checkpoint of CAR and IL-15 signalling in NK cells. Nature *643*, 1076–1086. https://doi.org/10.1038/s41586-025-09087-8.

40. Schmierer, B., and Hill, C.S. (2007). TGFβ–SMAD signal transduction: molecular specificity and functional flexibility. Nat. Rev. Mol. Cell Biol. *8*, 970–982. https://doi.org/10.1038/nrm2297.

41. Aykul, S., and Martinez-Hackert, E. (2016). Transforming Growth Factor-β Family Ligands Can Function as Antagonists by Competing for Type II Receptor Binding. J. Biol. Chem. *291*, 10792–10804. https://doi.org/10.1074/jbc.M115.713487.

42. Vuillefroy de Silly, R., Pericou, L., Seijo, B., Crespo, I., and Irving, M. (2024). Acidity suppresses CD8 + T-cell function by perturbing IL-2, mTORC1, and c-Myc signaling. EMBO J. *43*, 4922–4953. https://doi.org/10.1038/s44318-024-00235-w.

43. Tsherniak, A., Vazquez, F., Montgomery, P.G., Weir, B.A., Kryukov, G., Cowley, G.S., Gill, S., Harrington, W.F., Pantel, S., Krill-Burger, J.M., et al. (2017). Defining a Cancer Dependency Map. Cell *170*, 564–576.e16. https://doi.org/10.1016/j.cell.2017.06.010.

44. Wiedemann, G.M., Santosa, E.K., Grassmann, S., Sheppard, S., Le Luduec, J.B., Adams, N.M., Dang, C., Hsu, K.C., Sun, J.C., and Lau, C.M. (2021). Deconvoluting global cytokine signaling networks in natural killer cells. Nat. Immunol. *22*, 627–638. https://doi.org/10.1038/s41590-021-00909-1.

45. Peng, L., Renauer, P.A., Sferruzza, G., Yang, L., Zou, Y., Fang, Z., Park, J.J., Chow, R.D., Zhang, Y., Lin, Q., et al. (2025). In vivo AAV-SB-CRISPR screens of tumor-infiltrating primary NK cells identify genetic checkpoints of CAR-NK therapy. Nat. Biotechnol. *43*, 752–761. https://doi.org/10.1038/s41587-024-02282-4.

46. Gao, B., Kong, Q., Zhang, Y., Yun, C., Dent, S.Y.R., Song, J., Zhang, D.D., Wang, Y., Li, X., and Fang, D. (2017). The Histone Acetyltransferase Gcn5 Positively Regulates T Cell Activation. J. Immunol. *198*, 3927–3938. https://doi.org/10.4049/jimmunol.1600312.

47. Liao, X., Li, W., Zhou, H., Rajendran, B.K., Li, A., Ren, J., Luan, Y., Calderwood, D.A., Turk, B., Tang, W., et al. (2024). The CUL5 E3 ligase complex negatively regulates central signaling pathways in CD8+ T cells. Nat. Commun. *15*, 603. https://doi.org/10.1038/s41467-024-44885-0.

48. Cortez, J.T., Montauti, E., Shifrut, E., Gatchalian, J., Zhang, Y., Shaked, O., Xu, Y., Roth, T.L., Simeonov, D.R., Zhang, Y., et al. (2020). CRISPR screen in regulatory T cells reveals modulators of Foxp3. Nature *582*, 416–420. https://doi.org/10.1038/s41586-020-2246-4.

49. Loo, C.S., Gatchalian, J., Liang, Y., Leblanc, M., Xie, M., Ho, J., Venkatraghavan, B., Hargreaves, D.C., and Zheng, Y. (2020). A Genome-wide CRISPR Screen Reveals a Role for the Non-canonical Nucleosome-Remodeling BAF Complex in Foxp3 Expression and Regulatory T Cell Function. Immunity *53*, 143–157.e8. https://doi.org/10.1016/j.immuni.2020.06.011.

50. Paolino, M., Choidas, A., Wallner, S., Pranjic, B., Uribesalgo, I., Loeser, S., Jamieson, A.M., Langdon, W.Y., Ikeda, F., Fededa, J.P., et al. (2014). The E3 ligase Cbl-b and TAM receptors regulate cancer metastasis via natural killer cells. Nature *507*, 508–512. https://doi.org/10.1038/nature12998.

51. Kumar, B., Singh, A., Basar, R., Uprety, N., Li, Y., Fan, H., Cortes, A.K.N., Kaplan, M., Acharya, S., Shaim, H., et al. (2024). BATF is a major driver of NK cell epigenetic reprogramming and dysfunction in AML. Sci. Transl. Med. *16*, eadp0004. https://doi.org/10.1126/scitranslmed.adp0004.

52. Cortez, V.S., Ulland, T.K., Cervantes-Barragan, L., Bando, J.K., Robinette, M.L., Wang, Q., White, A.J., Gilfillan, S., Cella, M., and Colonna, M. (2017). SMAD4 impedes the conversion of NK cells into ILC1-like cells by curtailing non-canonical TGF-β signaling. Nat. Immunol. *18*, 995–1003. https://doi.org/10.1038/ni.3809.

53. Rea, A., Santana-Hernández, S., Villanueva, J., Sanvicente-García, M., Cabo, M., Suarez-Olmos, J., Quimis, F., Qin, M., Llorens, E., Blasco-Benito, S., et al. (2025). Enhancing human NK cell antitumor function by knocking out SMAD4 to counteract TGFβ and activin A suppression. Nat. Immunol. *26*, 582–594. https://doi.org/10.1038/s41590-025-02103-z.

54. Healy, L.P., Rossi, G.R., Rautela, J., Slade, C.A., Huntington, N.D., Winship, I.M., and Souza-Fonseca-Guimaraes, F. (2019). Loss-of-Function in SMAD4 Might Not Be Critical for Human Natural Killer Cell Responsiveness to TGF-β. Front. Immunol. *10*, 904. https://doi.org/10.3389/fimmu.2019.00904.

55. Krzywinska, E., Kantari-Mimoun, C., Kerdiles, Y., Sobecki, M., Isagawa, T., Gotthardt, D., Castells, M., Haubold, J., Millien, C., Viel, T., et al. (2017). Loss of HIF-1α in natural killer cells inhibits tumour growth by stimulating non-productive angiogenesis. Nat. Commun. *8*, 1597. https://doi.org/10.1038/s41467-017-01599-w.

56. Ni, J., Wang, X., Stojanovic, A., Zhang, Q., Wincher, M., Bühler, L., Arnold, A., Correia, M.P., Winkler, M., Koch, P.-S., et al. (2020). Single-Cell RNA Sequencing of Tumor-Infiltrating NK Cells Reveals that Inhibition of Transcription Factor HIF-1α Unleashes NK Cell Activity. Immunity *52*, 1075–1087.e1078. https://doi.org/10.1016/j.immuni.2020.05.001.

57. Garcia, J., Daniels, J., Lee, Y., Zhu, I., Cheng, K., Liu, Q., Goodman, D., Burnett, C., Law, C., Thienpont, C., et al. (2024). Naturally occurring T cell mutations enhance engineered T cell therapies. Nature *626*, 626–634. https://doi.org/10.1038/s41586-024-07018-7.

58. Dhaliwal, N.K., Weng, O.Y., Dong, X., Bhattacharya, A., Ahmed, M., Nishimura, H., Choi, W.W.Y., Aggarwal, A., Luikart, B.W., Shu, Q., et al. (2024). Synergistic hyperactivation of both mTORC1 and mTORC2 underlies the neural abnormalities of PTEN-deficient human neurons and

cortical organoids. Cell Rep. *43*, 114173. https://doi.org/10.1016/j.celrep.2024.114173.

59. Zhou, J., Wulfkuhle, J., Zhang, H., Gu, P., Yang, Y., Deng, J., Margolick, J. B., Liotta, L.A., Petricoin, E., and Zhang, Y. (2007). Activation of the PTEN/mTOR/STAT3 pathway in breast cancer stem-like cells is required for viability and maintenance. Proc. Natl. Acad. Sci. USA *104*, 16158–16163. https://doi.org/10.1073/pnas.0702596104.
60. Blaeschke, F., Chen, Y.Y., Apathy, R., Daniel, B., Chen, A.Y., Chen, P.A., Sandor, K., Zhang, W., Li, Z., Mowery, C.T., et al. (2023). Modular pooled discovery of synthetic knockin sequences to program durable cell therapies. Cell *186*, 4216–4234.e33. https://doi.org/10.1016/j.cell.2023.08.013.
61. Shy, B.R., Vykunta, V.S., Ha, A., Talbot, A., Roth, T.L., Nguyen, D.N., Pfeifer, W.G., Chen, Y.Y., Blaeschke, F., Shifrut, E., et al. (2023). High-yield genome engineering in primary cells using a hybrid ssDNA repair template and small-molecule cocktails. Nat. Biotechnol. *41*, 521–531. https://doi.org/10.1038/s41587-022-01418-8.
62. Nguyen, D.N., Roth, T.L., Li, P.J., Chen, P.A., Apathy, R., Mamedov, M.R., Vo, L.T., Tobin, V.R., Goodman, D., Shifrut, E., et al. (2020). Polymer-stabilized Cas9 nanoparticles and modified repair templates increase genome editing efficiency. Nat. Biotechnol. *38*, 44–49. https://doi.org/10.1038/s41587-019-0325-6.
63. Nguyen, E., Poli, M., Durrant, M.G., Thomas, A.W., Kang, B., Sullivan, J., Ng, M.Y., Lewis, A., Patel, A., Lou, A., et al. (2024). Sequence modeling and design from molecular to genome scale with Evo. Preprint at bioRxiv. https://doi.org/10.1101/2024.02.27.582234.
64. Ruffolo, J.A., Nayfach, S., Gallagher, J., Bhatnagar, A., Beazer, J., Hussain, R., Russ, J., Yip, J., Hill, E., Pacesa, M., et al. (2024). Design of highly functional genome editors by modeling the universe of CRISPR-Cas sequences. Preprint at bioRxiv. https://doi.org/10.1101/2024.04.22.590591.
65. Thean, D.G.L., Chu, H.Y., Fong, J.H.C., Chan, B.K.C., Zhou, P., Kwok, C. C.S., Chan, Y.M., Mak, S.Y.L., Choi, G.C.G., Ho, J.W.K., et al. (2022). Machine learning-coupled combinatorial mutagenesis enables resource-efficient engineering of CRISPR-Cas9 genome editor activities. Nat. Commun. *13*, 2219. https://doi.org/10.1038/s41467-022-29874-5.
66. Hamilton, J.R., Chen, E., Perez, B.S., Sandoval Espinoza, C.R., Kang, M. H., Trinidad, M., Ngo, W., and Doudna, J.A. (2024). In vivo human T cell engineering with enveloped delivery vehicles. Nat. Biotechnol. *42*, 1684–1692. https://doi.org/10.1038/s41587-023-02085-z.
67. Brinkman, E.K., Chen, T., Amendola, M., and van Steensel, B. (2014). Easy quantitative assessment of genome editing by sequence trace decomposition. Nucleic Acids Res. *42*, e168. https://doi.org/10.1093/nar/gku936.
68. Deng, J., Kang, Y., Cheng, C.C., Li, X., Dai, B., Katz, M.H., Men, T., Kim, M. P., Koay, E.A., Huang, H., et al. (2021). DDR1-induced neutrophil extracellular traps drive pancreatic cancer metastasis. JCI Insight *6*, e146133. https://doi.org/10.1172/jci.insight.146133.
69. Li, W., Xu, H., Xiao, T., Cong, L., Love, M.I., Zhang, F., Irizarry, R.A., Liu, J. S., Brown, M., and Liu, X.S. (2014). MAGeCK enables robust identification of essential genes from genome-scale CRISPR/Cas9 knockout screens. Genome Biol. *15*, 554.
70. Stuart, T., Butler, A., Hoffman, P., Hafemeister, C., Papalexi, E., Mauck, W. M., III, Hao, Y., Stoeckius, M., Smibert, P., and Satija, R. (2019). Comprehensive Integration of Single-Cell Data. Cell *177*, 1888–1902.e21. https://doi.org/10.1016/j.cell.2019.05.031.
71. Schneider, C.A., Rasband, W.S., and Eliceiri, K.W. (2012). NIH Image to ImageJ: 25 years of image analysis. Nat. Methods *9*, 671–675. https://doi.org/10.1038/nmeth.2089.
72. Kim, M.P., Li, X., Deng, J., Zhang, Y., Dai, B., Allton, K.L., Hughes, T.G., Siangco, C., Augustine, J.J., Kang, Y., et al. (2021). Oncogenic KRAS Recruits an Expansive Transcriptional Network through Mutant p53 to Drive Pancreatic Cancer Metastasis. Cancer Discov. *11*, 2094–2111. https://doi.org/10.1158/2159-8290.Cd-20-1228.
73. Henriksson, J., Chen, X., Gomes, T., Ullah, U., Meyer, K.B., Miragaia, R., Duddy, G., Pramanik, J., Yusa, K., Lahesmaa, R., and Teichmann, S.A. (2019). Genome-wide CRISPR Screens in T Helper Cells Reveal Pervasive Crosstalk between Activation and Differentiation. Cell *176*, 882–896.e18. https://doi.org/10.1016/j.cell.2018.11.044.
74. Ting, P.Y., Parker, A.E., Lee, J.S., Trussell, C., Sharif, O., Luna, F., Federe, G., Barnes, S.W., Walker, J.R., Vance, J., et al. (2018). Guide Swap enables genome-scale pooled CRISPR–Cas9 screening in human primary cells. Nat. Methods *15*, 941–946. https://doi.org/10.1038/s41592-018-0149-1.
75. Vera, J., Savoldo, B., Vigouroux, S., Biagi, E., Pule, M., Rossig, C., Wu, J., Heslop, H.E., Rooney, C.M., Brenner, M.K., and Dotti, G. (2006). T lymphocytes redirected against the κ light chain of human immunoglobulin efficiently kill mature B lymphocyte-derived malignant cells. Blood *108*, 3890–3897. https://doi.org/10.1182/blood-2006-04-017061.
76. Zhang, H., Zhang, Y., Zhou, X., Wright, S., Hyle, J., Zhao, L., An, J., Zhao, X., Shao, Y., Xu, B., et al. (2020). Functional interrogation of HOXA9 regulome in MLLr leukemia via reporter-based CRISPR/Cas9 screen. eLife *9*, e57858. https://doi.org/10.7554/eLife.57858.
77. Kolberg, L., Raudvere, U., Kuzmin, I., Adler, P., Vilo, J., and Peterson, H. (2023). g:Profiler—interoperable web service for functional enrichment analysis and gene identifier mapping (2023 update). Nucleic Acids Res. *51*, W207–W212. https://doi.org/10.1093/nar/gkad347.
78. Szklarczyk, D., Kirsch, R., Koutrouli, M., Nastou, K., Mehryary, F., Hachilif, R., Gable, A.L., Fang, T., Doncheva, N.T., Pyysalo, S., et al. (2023). The STRING database in 2023: protein-protein association networks and functional enrichment analyses for any sequenced genome of interest. Nucleic Acids Res. *51*, D638–D646. https://doi.org/10.1093/nar/gkac1000.
79. Ye, J., Coulouris, G., Zaretskaya, I., Cutcutache, I., Rozen, S., and Madden, T.L. (2012). Primer-BLAST: a tool to design target-specific primers for polymerase chain reaction. BMC Bioinf. *13*, 134. https://doi.org/10.1186/1471-2105-13-134.
80. Bernstein, N.J., Fong, N.L., Lam, I., Roy, M.A., Hendrickson, D.G., and Kelley, D.R. (2020). Solo: Doublet Identification in Single-Cell RNA-Seq via Semi-Supervised Deep Learning. Cell Syst. *11*, 95–101.e5. https://doi.org/10.1016/j.cels.2020.05.010.
81. Wolf, F.A., Angerer, P., and Theis, F.J. (2018). SCANPY: large-scale single-cell gene expression data analysis. Genome Biol. *19*, 15. https://doi.org/10.1186/s13059-017-1382-0.
82. Luecken, M.D., Büttner, M., Chaichoompu, K., Danese, A., Interlandi, M., Mueller, M.F., Strobl, D.C., Zappia, L., Dugas, M., Colomé-Tatché, M., and Theis, F.J. (2022). Benchmarking atlas-level data integration in single-cell genomics. Nat. Methods *19*, 41–50. https://doi.org/10.1038/s41592-021-01336-8.
83. Domínguez Conde, C., Xu, C., Jarvis, L.B., Rainbow, D.B., Wells, S.B., Gomes, T., Howlett, S.K., Suchanek, O., Polanski, K., King, H.W., et al. (2022). Cross-tissue immune cell analysis reveals tissue-specific features in humans. Science *376*, eabl5197. https://doi.org/10.1126/science.abl5197.
84. Hao, Y., Stuart, T., Kowalski, M.H., Choudhary, S., Hoffman, P., Hartman, A., Srivastava, A., Molla, G., Madad, S., Fernandez-Granda, C., and Satija, R. (2024). Dictionary learning for integrative, multimodal and scalable single-cell analysis. Nat. Biotechnol. *42*, 293–304. https://doi.org/10.1038/s41587-023-01767-y.
85. Bibby, J.A., Agarwal, D., Freiwald, T., Kunz, N., Merle, N.S., West, E.E., Singh, P., Larochelle, A., Chinian, F., Mukherjee, S., et al. (2022). Systematic single-cell pathway analysis to characterize early T cell activation. Cell Rep. *41*, 111697. https://doi.org/10.1016/j.celrep.2022.111697.

Please cite this article in press as: Biederstädt et al., Genome-wide CRISPR screens identify critical targets to enhance CAR-NK cell antitumor potency, Cancer Cell (2025), https://doi.org/10.1016/j.ccell.2025.07.021

CellPress
OPEN ACCESS

STAR★METHODS

KEY RESOURCES TABLE

REAGENT or RESOURCE	SOURCE	IDENTIFIER
Antibodies		
Brilliant Violet™ 605 anti-human CD56 (NCAM)	BioLegend	Cat# 318333; RRID: AB_11142683
Mouse Anti-Human CD3 Monoclonal Antibody, APC-H7 Conjugated	BD Biosciences	Cat# 560176; RRID: AB_1645475
Brilliant Violet™ 650 anti-human CD16	BioLegend	Cat# 302042; RRID: AB_2563801
PerCP/Cyanine5.5 anti-human CD45 (HI30)	BioLegend	Cat# 982312; RRID: AB_2810821
Brilliant Violet 785™ anti-human CD107a (LAMP-1) Antibody	BioLegend	Cat# 328644, RRID: AB_2565968
Spark YG 581 anti-CD56 (QA17A16)	BioLegend	Cat#: 392430, RRID: AB_2890829
BUV 661 anti-DNAM-1 (DX11)	BD	Cat#: 749934, RRID: AB_2917646
BV 570 anti-CD16 (3G8)	BioLegend	Cat#: 302036, RRID: AB_2632790
APC CY7 anti-2B4 (CD244) (C1.7)	BioLegend	Cat#: 329518, RRID: AB_2572015
BUV 805 anti-CD25 (2A3)	BD	Cat#: 742070, RRID: AB_2871356
APC FIRE 810 anti-CD3 (SK7)	BioLegend	Cat#: 344858, RRID: AB_2860895
BV 785 anti-CD2 (RPA-2.10)	BioLegend	Cat#: 300234, RRID: AB_2800717
PE-DAZZLE 594 anti-CD57 (HNK-1)	BioLegend	Cat#: 359620, RRID: AB_2564063
NB610 anti-CD62L (DREG56)	Thermo Fisher	Cat#: 368-0629-42, RRID: AB_2896126
AF532 anti-CD69 (FN50)	Novus Biologicals	Cat#: NBP1-43387AF532, RRID: N/A
BV510 anti-CD95L (CD178) (NOK-1)	BD	Cat#: 744098, RRID: AB_2741992
PERCP anti-CD161 (KLRB1) (HP-3G10)	BioLegend	Cat#: 339934, RRID: AB_2563999
BUV 563 anti-ICOS (DX29)	BD	Cat#: 568215, RRID: AB_2916844
PE-FIRE 810 anti-KLRG1 (SA231A2)	BioLegend	Cat#: 367733, RRID: AB_289462
SB702 anti-LAG3 (3DS223H)	Thermo Scientific	Cat#: 67-2239-42, RRID: AB_2802457
PE-CY5 anti-NKG2A (S19004C)	BioLegend	Cat#: 375112, RRID: AB_2888864
FITC anti-NKG2C (134591)	R&D	Cat#: FAB138G, RRID: N/A
BV750 anti-NKG2D (1D11)	BD	Cat#: 747025, RRID: AB_2871796
BUV737 anti-NKP30 (p30-15)	BD	Cat#: 749128, RRID: AB_2873517
PE CY5.5 anti-NKP44 (1G6)	Novus Biologicals	Cat#: NBP2-42683PECY55, RRID: N/A
PE CY7 anti-NKP46 (9E2)	Thermo Scientific	Cat#: 25-3359-42, RRID: AB_2573444
PE-AF700 anti-TRAIL (2E5)	AAT Bioquest	Cat#: 125301X1, RRID: N/A
BV605 anti-PD-1 (EH12.1)	BD	Cat#: 563245, RRID: AB_2738091
BUV496 anti-CD8a (RPA-T8)	BD	Cat#: 612943, RRID: AB_2916884
BV650 anti-TIGIT (741182)	BD	Cat#: 747840, RRID: AB_2872303
PerCP eFluor 700 anti-CD96 (NK92.39)	Thermo Fisher	Cat#: 46-0969-42, RRID: AB_2573702
BUV 615 anti-TIM-3 (7D3)	BD	Cat#: 752363, RRID: AB_2875880
BV 480 anti-OX40 (CD134) (ACT35)	BD	Cat#: 746649, RRID: AB_2743926
BUV 395 anti-CD14 (MϕP9)	BD	Cat#: 569102, RRID: AB_2744288
BUV 395 anti-CD33 (P67.6)	BD	Cat#: 745709, RRID: AB_2743189
SparkNIR 685 anti-CD45 (2D1)	BioLegend	Cat#: 368552, RRID: AB_2820026
UV Ghost 450 anti-L/D ()	Tonbo	Cat#: 13-0868-T100, RRID: N/A
PE anti-PANKIR (DX9)	BD	Cat#: 340484, RRID: AB_400041
BB700 anti-CXCR6 (13B 1E5)	BD	Cat#: 745882, RRID: AB_2743316
BUV395 anti-CD19 (SJ25C1)	BD	Cat#: 563551, RRID: AB_2738272

(*Continued on next page*)

Please cite this article in press as: Biederstädt et al., Genome-wide CRISPR screens identify critical targets to enhance CAR-NK cell antitumor potency, Cancer Cell (2025), https://doi.org/10.1016/j.ccell.2025.07.021

Continued

REAGENT or RESOURCE	SOURCE	IDENTIFIER
Bacterial and virus strains		
XL1-Blue Supercompetent Cells	Agilent Technologies, Inc.	Cat# 200236
NEB 5-alpha Competent E. coli (High Efficiency)	New England Biolabs	Cat# C2987H
Biological samples		
Human cord blood-derived natural killer cells	The University of Texas MD Anderson Cancer Center Cord Blood Bank	IRB-approved protocol Lab04-0249
Chemicals, peptides, and recombinant proteins		
Alt-R™ S.p. Cas9 Nuclease V3	Integrated DNA Technologies	Cat# 10000735
Alt-R® Cas9 Electroporation Enhancer	Integrated DNA Technologies	Cat# 1075916
Recombinant Human TGF-β1 (carrier-free)	Biolegend	Cat# 781804
L-(+)-Lactic acid	Sigma-Aldrich	Cat# L1750-10G
LIVE/DEAD™ Fixable Green Dead Cell Stain Kit, for 488 nm excitation	ThermoFisher Scientific	Cat# L34970
CD235a (Glycophorin A) MicroBeads, human	Miltenyi Biotec	Cat# 130-050-501
Lymphoprep	STEMCELL	Cat# 07861
Antibiotic-Antimycotic (100X)	ThermoFisher Scientific	Cat# 15240062
RPMI 1640 Medium	Gibco	Cat# 11995073
Click's Medium (EHAA)	Fujifilm	Cat# 9195
OptiMEM	Gibco	Cat# 31985070
GlutaMAX	Gibco	Cat# 35050061
Human recombinant interleukin-2	PROLEUKIN® (Aldesleukin)	https://www.accessdata.fda.gov/drugsatfda_docs/label/2012/103293s5130lbl.pdf
Retro-X Concentrator	Takara Bio	Cat# PT5063-2
DNAse I	ThermoFisher Scientific	Cat# EN0521
Critical commercial assays		
NK Cell Isolation Kit, human	Miltenyi Biotec	Cat# 130-092-657
P3 Primary Cell 4D-Nucleofector® X Kit L	LONZA	Cat# V4XP-3024
DNeasy Blood and Tissue Kits for DNA Isolation	QIAGEN	Cat # 69504
Agilent Technologies E-PLATE 96 well xCELLigence	Agilent Technologes, Inc.	Cat# NC1610670
Deposited data		
Western blotting source image files	This paper	Zenodo: [https://doi.org/10.5281/zenodo.15879918]
Guide and gene level MAGeCK results of transcription factor library CRISPR screen in primary human NK cells	This paper	Table S1
Guide and gene level MAGeCK results of genome-wide CRISPR screen in primary human NK cells	This paper	Table S1
Single cell RNA seq data of CRISPR-edited primary human NK cells	This paper	Zenodo: [https://doi.org/10.5281/zenodo.15802140]
Experimental models: Cell lines		
HEK293T	Takara Bio	Cat #632180
Panc1	ATCC	Cat# CRL-1469
MDA-PATC 148	The University of Texas MD Anderson Cancer Center[68]	N/A
Capan-1	ATCC	Cat# HTB-79
MM1S	ATCC	Cat# CRL-2974
THP-1	ATCC	Cat# TIB-202

(*Continued on next page*)

Please cite this article in press as: Biederstädt et al., Genome-wide CRISPR screens identify critical targets to enhance CAR-NK cell antitumor potency, Cancer Cell (2025), https://doi.org/10.1016/j.ccell.2025.07.021

Continued

REAGENT or RESOURCE	SOURCE	IDENTIFIER
WiDR	ATCC	CCL-218
OVCAR-5	Millipore Sigma	SCC259
MOLM-14	DSZM	Cat# ACC 777
Experimental models: Organisms/strains		
Mouse: NOD.Cg-Prkdcscid Il2rgtm1Wjl/SzJ	The Jackson Laboratory	RRID: IMSR_JAX:005557
Oligonucleotides		
MED12 sgRNA Guide_#4: TTCACATTATGACCAACACC	Cellecta, Inc.	Cat# KOHGW-80Kv2-P https://cellecta.com
ARIH2 sgRNAs Guide_#1: AGACGACCCUGGGGACAUAG Guide_#2: CUGGUACUCCUCGGGAUCAA Guide_#3: GGGGUCUGACAGCAAUGAAG	EditCo Bio, Inc. (formerly Synthego)	Gene Knockout Kit – human – ARIH2
CCCN sgRNAs Guide_#1: AUUGGUUCAAAUUGUAUAGU Guide_#2: AGAGAAACUUUAAAUCCUUU Guide_#3: UUCUAGUUUGCAAUGGAUUU	EditCo Bio, Inc. (formerly Synthego)	Gene Knockout Kit – human – CCNC
Recombinant DNA		
Teichmann pMSCV-U6sgRNA(Bbsl)-PGKpuro2ABFP retroviral sgRNA transfer plasmid	Addgene	Cat# 102796
CRISPR Human Genome 80K Knockout Library	Cellecta, Inc.	KOHGW-80Kv2-P
Software and algorithms		
MAGeCK	Li et al.[69]	https://sourceforge.net/p/mageck/wiki/Home/
Seurat	Stuart et al.[70]	
OMIQ	Dotmatics	https://www.dotmatics.com/solutions/omiq
Morpheus	Broad Institute	https://clue.io/morpheus https://software.broadinstitute.org/morpheus
FlowJo version 10.10	Becton Dickinson & Company (BD)	https://www.flowjo.com/
ImageJ	Schneider et al.[71]	
PRISM version 10.4.0	GraphPad Software, LLC	https://www.graphpad.com
bioRender	Biorender	https://www.biorender.com
Adobe Illustrator 2025 version 29.0.1	Adobe Inc.	https://www.adobe.com/
TIDE: Tracking of Indels by DEcomposition	Brinkman et al.[67]	http://shinyapps.datacurators.nl/tide/

EXPERIMENTAL MODEL AND STUDY PARTICIPANT DETAILS

Mouse models

All procedures and experimental protocols involving mice were approved by the Institutional Animal Care and Use Committee (IACUC) protocol number 00001263-RN01 at The University of Texas MD Anderson Cancer Center (Houston, TX). We used 8 to 10-week-old female NOD/SCID IL-2Rγnull (NSG) mice for xenograft model for our mice experiments to assess the antitumor activity of CRISPR KO CAR NK cells *in vivo*.

Cancer cell lines

Human pancreatic cancer cell lines Panc1 (CRL-1469), Capan-1 (Cat# HTB-79), CFPAC (CRL-1918) and 293T (Cat# CRL-3216) were obtained from the American Type Culture Collection (ATCC). PATC148 was a gift from Dr. Anirban Maitra (MD Anderson Cancer Center).[72] Panc1 and PATC148 were cultured in DMEM medium (Gibco, Cat# 11965092), supplemented with 10% FBS (Corning; Cat# 9035535) and 1% Antibiotic-Antimycotic (Gibco; Cat# 15240062). CFPAC cells were cultured in IMDM medium (Gibco; Cat# 12440053), supplemented with 10% fetal bovine serum (FBS; Corning; Cat# 9035535) and 1% Antibiotic-Antimycotic (Gibco; Cat# 15240062). Capan-1 cells were cultured in IMDM medium (Gibco; Cat# 12440053), supplemented with 20% FBS (Corning; Cat# 9035535), 1% Antibiotic-Antimycotic (Gibco; Cat# 15240062). 293T cells were cultured in DMEM media (Gibco, Cat# 11965092) with 10% FBS (Corning; Cat# 9035535) and 1% Antibiotic-Antimycotic (Gibco; Cat# 15240062). Human metastatic

gastrointestinal cancer cell line OVCAR-5 was obtained from Sigma-Aldrich (Cat# SCC259) and cultured in RPMI-1640 medium (Gibco; Cat# 11875093), supplemented with 10% FBS (Corning; Cat# 9035535) and 1% Antibiotic-Antimycotic (Gibco; Cat# 15240062) and 1% GlutaMAX (Gibco; Cat# 35050061). K562 cells (CCL-243) were bought from the American Type Culture Collection (ATCC) and cultured in RPMI-1640 medium (Gibco; Cat# 11875093), supplemented with 10% FBS (Corning; Cat# 9035535) and 1% Antibiotic-Antimycotic (Gibco; Cat# 15240062) and 1% GlutaMAX (Gibco; Cat# 35050061). Human acute myeloid leukemia cell lines THP1 (Cat# TIB-202) and MOLM-14 (Cat# ACC 777) were obtained from the American Type Culture Collection (ATCC) and the German Collection of Microorganisms and Cell Cultures GmbH (DSMZ), respectively, and cultured in RPMI-1640 medium (Gibco; Cat# 11875093), supplemented with 10% FBS (Corning; Cat# 9035535) and 1% Antibiotic-Antimycotic (Gibco; Cat# 15240062) and 1% GlutaMAX (Gibco; Cat# 35050061). Human Karpas 299 T cell non-Hodgin's lymphoma cell line was purchased from Sigma-Aldrich (Cat# 06072604) and cultured in RPMI-1640 media (Gibco; Cat# 11875093) with 10% FBS, 1% GlutaMAX (Gibco; Cat# 35050061), 1% Antibiotic-Antimycotic (Gibco; Cat# 15240062). UMRC3 cell line was obtained from Sigma-Aldrich (Cat# 08090512) and cultured in EMEM media with 10% FBS (Corning; Cat# 9035535), 1% GlutaMAX (Gibco; Cat# 35050061), 1% non-essential amino acids (Sigma-Aldrich; Cat# M7145), 1% Antibiotic-Antimycotic (Gibco; Cat# 15240062). The breast cancer PDX cell line BCX-010 was kindly provided by Dr. Funda Meric-Bernstam at MD Anderson Cancer Center (MDACC) and cultured in DMEM medium (Gibco, Cat# 11965092), supplemented with 10% FBS (Corning; Cat# 9035535) and 1% Antibiotic-Antimycotic (Gibco; Cat# 15240062). All cell lines were authenticated with STR profiling at the MD Anderson Cancer Center Cell Line Characterization Core Facility and routinely tested for Mycoplasma negativity.

Primary human NK cells

Isolation and expansion of cord blood-derived NK cells (CB-NK) were carried out using cord blood units obtained from the MD Anderson Cancer Center (MDACC) cord blood bank under an IRB-approved protocol (Lab04-0249). The process involved isolating and expanding CB-NK cells according to previously described methods.[3] In brief, lymphocytes were collected by using Ficoll-Histopaque solution (Sigma-Aldrich) through density-gradient centrifugation. Subsequently, $CD56^{+}CD3$- NK cells were purified by negative selection using the Miltenyi Biotec NK cell isolation kit (Catalog number: 130-092-657) according to the manufacturer's protocol. Isolated NK cells were subsequently co-cultured with irradiated (100 Gy) universal antigen presenting cells (uAPCs) at a 1:2 ratio in appropriate cell culture medium (50% 1640 RPMI, 50% Click's medium, 10% FBS, 1% Antibiotic-Antimycotic, 1% GlutaMAX) supplemented with 200 U/ml recombinant human IL-2 (Proleukin, 400U/mL; Chiron, Emeryville, CA, USA).

METHOD DETAILS

Cloning of viral constructs

We obtained the pMSCV-U6sgRNA(Bbsl)-PGKpuro2ABFP[73] from Sarah Teichmann (Addgene plasmid # 102796) and modified it to express a specific sgRNA using standard molecular cloning techniques. To validate targeted genomic disruption using retroviral sgRNA delivery paired with Cas9 transfection by electroporation, a previously validated sgRNA (*PTPRC* (CD45) sgRNA_C: GAGGATCCTCAGGCACCCCG) targeting the canonical NK cell surface marker *PTPRC* (CD45)[74] was cloned into the sgRNA transfer plasmid under the control of the U6 promoter.

Retroviral production

HEK 293T cells were plated in 15 cm dishes one day prior to transfection and cultured in DMEM medium, supplemented with 10% FBS and 1% GlutaMAX (Gibco; Cat# 35050061). HEK 293T were transfected at 70-80% confluency with the pMSCV_U6sgRNA (Bbsl)-PGKpuro2ABFP expression vector (Addgene: Plasmid #102796) along with packaging and envelope plasmids using the FuGENE® HD Transfection Reagent (Cat# E2312) as previously described.[75] The following day, media was replaced with OptiMEM medium supplemented with 10% FBS, 1% GlutaMAX (Gibco; Cat# 35050061), 0.5% Antibiotic-Antimycotic (Gibco; Cat# 15240062), DNAse I (1 U/mL) (ThermoFisher; Cat# EN0521), 5mM $MgCl_2$, 1mM sodium pyruvate (Gibco; Cat# 11360070) and 1x MEM nonessential amino acids (Gibco; Cat# 11140050). Viral supernatant was collected 48h and 72h post transfection, filtered to remove cellular debris and frozen at -80C. Retroviral particles were concentrated using Retro-X™ concentrator (Takara, Cat# 631456) according to the manufacturer's protocol and resuspended at 1% of the original volume for enhanced titer.

CRISPR editing of primary human NK cells using retroviral sgRNA transfer and Cas9 electroporation

Primary human NK cells were transduced on day 5 post-isolation using the retroviral sgRNA transfer plasmid containing a specific sequence targeting *PTPRC* (CD45). Following transduction, NK cells were electroporated on d7 using the Lonza 4D nucleofector X unit (Cat #AAF-1003X). NK cells were washed with PBS, pelleted, and resuspended in P3 primary buffer, supplemented with Cas9 (10.16μM; Alt-R™ S.p. Cas9 Nuclease V3, Integrated DNA Technologies, Cat# 10000735) and electroporation enhancer (4.16μM; Alt-R™ Cas9 Electroporation Enhancer, Integrated DNA Technologies, Cat# 1075916), at a density of 1 x 10^6 cells/20μL. NK cells were transferred into Lonza electroporation 16-well Nucleocuvettes (P3 Primary Cell 4D-Nucleofector™ X Kit S, Lonza Bioscience, Cat# V4XP-3032) and electroporated using pulse code CM137. Post electroporation, NK cells were recovered with 100μL prewarmed NK cell medium and rested for 10-15 minutes in the incubator at 37C. NK cells were then transferred to cell culture flasks containing irradiated uAPC cells at an E:T ratio of 1:2, suspended in prewarmed NK cell medium, supplemented with IL-2 (400U/mL). Starting on

Please cite this article in press as: Biederstädt et al., Genome-wide CRISPR screens identify critical targets to enhance CAR-NK cell antitumor potency, Cancer Cell (2025), https://doi.org/10.1016/j.ccell.2025.07.021

day 12 post-isolation, NK cells which had stably integrated the sgRNA transfer vector, were selected with puromycin (2.5μg/mL) for 6 days. Knockout of *PTPRC* (CD45) was confirmed using flow cytometry.

Transcription factor library assembly

The human transcription factor knockout library was derived from the Lenti-human-TF-gRNA puromycin library (Addgene #162275), targeting 1,639 transcription factors and comprising 11,364 sgRNAs, with 7 sgRNAs per gene and 100 non-targeting controls.[76] The library was cloned into the retroviral construct pMSCV-U6sgRNA(BbsI)-PGKpuro2ABFP (Addgene plasmid # 102796) following adaptation to a previously published cloning method.[73] The library was amplified by polymerase chain reaction (PCR), and the pMSCV backbone was digested with BamHI-HF (New England Biolabs, #R3136L). HiFi DNA assembly of the library amplicon into pMSCV was performed at 50°C for 1 hour in a 20 μl reaction with 100 ng digested backbone, 11 ng amplified insert (2:1 molar ratio of insert to backbone), and HiFi DNA Assembly Master Mix (New England Biolabs, #M5520). HiFi reactions were purified using isopropanol precipitation, and 2 μl of the purified product was transformed into Endura™ Electrocompetent Cells (Lucigen, #60242-1) using a BioRad MicroPulser with 0.1 cm gap cuvettes (Bio-Rad, #1652089). Transformed cells were cultured overnight, and plasmids were isolated using the Purelink™ HiPure Plasmid Filter Midi prep Kit (Thermo Scientific, K210015). Guide representation was confirmed by sequencing using Illumina MiSeq V3-150.

Transcription factor library CRISPR screens in primary human NK cells

Primary human NK cells were retrovirally transduced with a transfer plasmid containing the transcription factor library (11,364 unique sgRNAs) on day 5 post isolation from cord blood. NK cells which had stably integrated a copy of the vector plasmid following low-MOI (0.3) transduction were subsequently selected using puromycin at a concentration of 2.5μg/mL. On day 11, library-transduced NK cells were electroporated with recombinant Cas9 protein (18.3μM, Alt-R™ S.p. Cas9 Nuclease V3, Cat# 1081059) in the presence of P3 primary buffer using the Lonza 4D Nucleofector (P3 Primary Cell 4D-Nucleofector X Kit L, Cat # V4XP-3012). Immediately after electroporation, NK cells were recovered using prewarmed NK cell medium, rested in the incubator for 10-15min at 37C and subsequently re-expanded with uAPCs at an E:T ratio of 1:1. T0 samples were collected on day 15.

On day 18, NK cells, were split into four different screening conditions. For the NK cell expansion screens, TF-library-edited NK cells were cultured in NK cell medium, supplemented with IL-2 (200U/L) with and without irradiated uAPCs (E:T=1:2). For the pancreatic cancer re-challenge screens, NK cells were co-cultured with the human pancreatic cancer cell lines Panc-1 and PATC-148 at an initial E:T of 8:1. NK cells were re-challenged by adding $1x10^6$ of the respective tumor cells every three days and harvested on day 12. Changes in relative sgRNA abundance were assessed compared to T0 by next-generation sequencing (NGS).

Transcription factor library sequencing

For TF library screens, 10 million cells from each sample were harvested on T12 after removing dead cells using the Dead Cell Removal Kit (Miltenyi Biotec, 130-090-101). Genomic DNA was extracted from the cell pellets using the QIAamp DNA Blood Midi Kit (Qiagen, 51185). Integrated sgRNA sequences were amplified and barcoded following a two-step PCR protocol (Olivieri & Durocher, STAR Protocols 2, 100321, March 19, 2021). For the first PCR, a total of 18 μg of genomic DNA was divided across six reactions with Q5 Hot Start High-Fidelity 2X Master Mix (NEB #M0494L). The PCR products were pooled together for each sample and purified using the QIAquick PCR Purification Kit (QIAGEN, 28104). The purified product was then further PCR-amplified with i5 and i7 index primers. The libraries were purified using the QIAquick Gel Extraction Kit (Qiagen, 28704) and then run on a High Sensitivity D1000 tape (Agilent). Sequencing was performed on a NextSeq500 instrument to a targeted depth of 5.2 x 10e6 reads per sample.

Primer list

TF library amplification primer

F: 5′- tcttacgtagctagcggatcccgaggggacccagagagg -3’

R: 5′- ctacccggtagaattggatccaaaaaaagcaccgactcggtg -3’

Two-step PCR; first PCR primer

F: 5′-gagggcctatttcccatgattc-3’

R: 5′-tgctaaagcgcatgctccagac-3’

Two-step PCR; second PCR primer

F: 5′-AATGATACGGCGACCACCGAGATCTACAC [i5 index] ACACTCTTTCCCTACACGACGCTCTTCCGATCTTTGTGGAAAGG ACGAAACACC-3’

R: 5′- CAAGCAGAAGACGGCATACGAGAT [i7 index] GTGACTGGAGTTCAGACGTGTGCTCTTCCGATCTACTTGCTATTTCTA GCTCTAAAAC-3’

Pooled genome-wide CRISPR screening in primary human NK cells

To investigate NK cell regulators at genome-wide scale, we obtained a genome-wide sgRNA library containing 77,736 unique sgRNA sequences targeting a total of 19,281 genes along with 500 non-targeting control guides from a commercial vendor (Cellecta, Inc.). Cloning of the genome-wide library into the pMSCV-U6sgRNA(BbsI)-PGKpuro2ABFP vector was performed by Cellecta, Inc. (320 Logue Ave. Mountain View, CA 94043 USA).

On day 5 post isolation, primary human NK cells from each donor were transduced with the retroviral vector expressing the genome-wide sgRNA library at low MOI (0.3) at a coverage $\geq$ 500x in RetroNectin-coated plates (Takara, Cat# T100B). Starting

day 7, NK cells stably expressing the CRISPR library vector, were selected using puromycin (Gibco; Cat# A1113803) at a concentration of 2.5μg/mL for a duration of 5 days, replenishing puromycin every 48h. Puromycin-selected NK cells were transfected with Cas9 by electroporation using the Lonza 4D nucleofector device. In brief, NK cells were washed with PBS, pelleted, and resuspended in P3 primary buffer, supplemented with Cas9 (10.16μM; Alt-R™ S.p. Cas9 Nuclease V3, Integrated DNA Technologies, Cat# 10000735) and electroporation enhancer (4.16μM; Alt-R™ Cas9 Electroporation Enhancer, Integrated DNA Technologies, Cat# 1075916), at a density of 1 x 10^7 cells/100μL. NK cells were transferred into Lonza electroporation Nucleocuvettes (P3 Primary Cell 4D-Nucleofector™ X Kit L, Lonza Bioscience, Cat# V4XP-3024) and electroporated using pulse code CM137. After electroporation, NK cells were recovered with 500μL prewarmed NK cell medium and rested for 10-15 minutes in the incubator at 37C. Subsequently, NK cells transferred to cell culture flasks containing irradiated uAPC cells suspended in prewarmed NK cell medium, supplemented with IL-2 (400U/mL). NK cells were re-expanded with irradiated uAPCs at a 1:1 ratio for 6 days. Flow cytometry was used to determine library vector integration, purity after puromycin selection and NK cell purity. Library coverage was maintained at $\geq$ 500x throughout the entire editing pipeline.

Genome-wide tumor re-challenge CRISPR screens in primary human NK cells

After completion of puromycin selection, T0 samples of the genome-wide CRISPR library-edited NK cells were harvested, pelleted and frozen at -80C. NK cells were then co-cultured with human pancreatic cancer cell line Capan-1 at an initial effector-to-target (E:T) ratio of 1:1 in the presence of IL-2 (400U/mL). NK cells were re-challenged with two additional rounds of Capan-1 pancreatic tumor cells at an E:T ratio of 4:1. CRISPR library-edited NK cells were propagated to maintain screen coverage at $\geq$ 500x throughout the entire assay duration and harvested after 14 days of repeated tumor challenges. Changes in relative sgRNA abundance were assessed compared to T0 by next-generation sequencing (NGS).

Genome-wide degranulation screen in primary human NK cells

NK cells, transduced with the genome-wide library, were challenged with two rounds of Capan-1 pancreatic cancer cells at E:T ratios of 1:1 and 4:1, respectively. On day 9, NK cells were challenged with another round of tumor cells at an E:T ratio of 2:1 while adding anti-human CD107a (Lamp-1) antibody (BioLegend; H4A3, Cat# 328644) directly into the culture medium at a concentration of 10μL/mL. NK cells were harvested after 2h, washed and stained using the following antibodies: LIVE/DEAD™ Fixable Green Dead Cell Stain Kit (Thermofisher; Cat# L34969), CD107a (Lamp-1) antibody (BioLegend; H4A3, Cat# 328644). NK cells were subsequently sorted into two bins based on the tail-end fractions with the highest and lowest CD107a expression levels, respectively. Sorted NK cells were pelleted and frozen at -80C before extraction of genomic DNA and assessment of altered sgRNA distribution by NGS. Sorting of primary human NK cell performed at the MD Anderson Cancer Center Flow Cytometry and Cellular Imaging Core Facility using the BD Aria II Cell Sorter.

Genome-wide immuno-metabolite CRISPR screens in primary human NK cells

After puromycin selection, CRISPR library-edited NK cells were re-expanded with two rounds of uAPCs at an E:Tratio of 1:2 and 1:1, respectively, in the presence of IL-2 (400U/mL)for a total duration of 14 days. NK cells were concomitantly exposed to specific TME-associated immuno-metabolites at defined doses (L(+)-lactic acid: 5mM; TGFβ1 (Biolegend Cat#781804): 500ng/mL) or hypoxia (4% O2). On day 14, NK cells were harvested and relative sgRNA composition was assessed through deep sequencing.

Next-generation sequencing and bioinformatic analyses

Extraction of genomic DNA from cell pellets and next-generation sequencing services were performed by Cellecta, Inc. (320 Logue Ave. Mountain View, CA 94043 USA). MAGeCK[69] scores were computed comparing d14 versus T0 guide distribution for the different screening conditions using default settings and paired analysis. NK cell donors were analyzed in aggregate. Where indicated, MAGeCK-computed gene-level log2 fold changes (LFC) were transformed to obtain LFC z scores (ZS).

Functional annotation of screen hits

Functional annotation of positive screen hits (FDR<0.05, |ZS|>1.5) was performed based on the following curated ontologies: GO_CC: Cul5-RING ubiquitin ligase complex (GO:0031466), GO_CC: CKM complex (GO:1990508), GO_CC: SAGA complex (GO:0000124), GO_BP: Negative regulation of NFkappaB Transcription factor activity (GO:0032088), GO_BP: Chromatin remodeling (GO:0006338), GO_MF: DNA-binding transcription factor activity (GO:0003700). The following pathways were manually addended based on functional affinity: GO_CC: CKM complex (GO:1990508): *PTEN* (Mediator kinase module & regulation of RNA Polymerase II), GO_CC: Cul5-RING ubiquitin ligase complex (GO:0031466): *RNF7*, *CISH*, *SOCS1-5* (Cul5-RING ubiquitin ligase complex + SH-domain containing family interactions partners).

Pathway overrepresentation analysis

Pathway overrepresentation of detected screen hits in curated gene sets was performed using g:Profiler (Version e111_eg58_p18_30541362) with Bonferroni multiple testing correction applying a significance threshold of 0.05 (https://biit.cs.ut.ee/gprofiler/gost).[77]

Please cite this article in press as: Biederstädt et al., Genome-wide CRISPR screens identify critical targets to enhance CAR-NK cell antitumor potency, Cancer Cell (2025), https://doi.org/10.1016/j.ccell.2025.07.021

Protein-protein interaction mapping

Top screen hits (FDR<0.05; |ZS|>1.5) from the genome-wide Capan-1 re-challenge screen in primary human NK cells were uploaded into the STRING database and edges were generated by projected protein-protein interactions.[78] Nodes were clustered using K-means clustering and subsequently functionally annotated according to biological function using GO terms and manual curation.

Flow cytometry and cell sorting

NK cell viability was determined with LIVE/DEAD™ Fixable Green Dead Cell Stain Kit (Thermofisher; Cat# L34969). Stable integration of the sgRNA transfer plasmid as well as purity after puromycin selection was assessed by detection of blue fluorescent protein (BFP) reporter as previously described.[73]

The following antibodies were used for flow cytometry experiments: BV785 anti-human CD107a (Lamp-1) (BioLegend, H4A3, Cat# 328644), APC-Cy7 anti-human CD3 (BioLegend, HIT3a, Cat# 300318), BV605 anti-human CD56 (BioLegend, HCD56, Cat# 318334), BV650 anti-human CD16 (BD Biosciences, 3G8, Cat# 563173), PerCP anti-human CD45 (BioLegend, HI30, Cat# 304026), APC-Cy7 anti-human CD45 (BioLegend, HI30, Cat# 304014), AF-700 anti-mouse CD45 (BioLegend, QA17A26, Cat# 157616), PE-CF594 anti-human CD27 (BD Biosciences, M-T271, Cat# 562297), PE-Cy7 anti-human CD70 (Biolegend, 113-16, Cat# 355112), AF-700 anti-mouse CD45 (Biolegend, QA17A26, Cat# 157616), PE anti-human TROP2 (Biolegend, NY18, Cat# 363804), Anti-His-APC (Biolegend, J095G46, Cat# 362605), PE anti-human CD326 (EpCAM; Biolegend, 9C4, Cat# 324206), and FITC anti-human CD326 (EpCAM; Biolegend, 9C4, Cat# 324204). Cytometric data were acquired using a LSRFortessa (BD Biosciences) and analyzed using FlowJo (Version 10.10.0) and Omiq (Dotmatics). Fluorescense-based cell sorting was performed on a high-throughput BD Biosciences Aria II Cell Sorter Cell Sorter at the MDACC North Campus Flow Cytometry and Cellular Imaging Core Facility.

Spectral flow cytometry

After co-culture with Capan-1 pancreatic cancer cell lines for 7 days, NK cells were harvested, washed and stained with a multi-parameter antibody cocktail. The antibodies used for spectral flow cytometry experiments are listed in the key resources table. Spectral flow cytometric analysis was performed using the ID7000™ Spectral Cell Analyzer (Sony Biotechnology Inc., San Jose, CA, USA). Spectral unmixing and data analysis was performed using the Sony ID7000™ software suite. Semi-supervised clustering was performed using FlowSOM and dimensionality reduction was performed using opt-SNE algorithm by OMIQ (Dotmatics). The median expression of each marker was normalized using Z-score, then hierarchically clustered (1-Pearson), and plotted as a heatmap with the percentage positivity overlayed for each marker using Morpheus matrix visualization and analysis software (Broad Institute).

Prioritization of screen hits for functional validation

Top screen hits (rank<100) originating from the five genome-wide CRISPR screens in primary human NK cells were prioritized for further *in vitro* and *in vivo* functional validation based on a weighed scoring algorithm including the number of overlaps across performed screens and their previously established role in NK cell biology. Additional weight was assigned to screen hits originating from the genome-wide NK cell:Capan-1 re-challenge screen under the assumption that cell fitness advantages conferred by these screen hits would directly be associated with improved antitumor killing capacity. In addition, screen hits involving genes described to be tumor suppressors were given additional weight with the rational of exploiting naturally occurring acquired cell fitness advantages of transformed cells in line with recent evidence.[57]

In brief, top hits (rank<100) from each screen (Table S2) were given a rank-based score (100/rank). The rank score for hits originating from the NK cell:Capan-1 cell screen was overweighted to match the combined weight of hits resulting from the three immunometabolite pressures screens (3:1:1:1 ratio). Screen hits which had previously been described to negatively impact immune cell function as well as hits previously characterized to improve NK cell function were filtered to focus on previously unrecognized regulators. Known tumor suppressor genes were assigned a 1.5x cofactor and hits with >3 screen overlaps were weighted at 1.75x to account for their presumably higher likelihood of conferring cell fitness advantages which enhance antitumor potency and protect against a variety of clinically relevant immunosuppressive conditions. Combined screen hits were ranked according to their weighted scores and the top three prioritized hits (*MED12*, *ARIH2* and *CCNC*) were prioritized for further validation.

CRISPR/Cas9-RNP editing of primary human NK cells

Validation of selected screen hits was performed by electroporating primary human NK cells with CRISPR-ribonucleoproteins (RNP) targeting *MED12*, *ARIH2* and *CCNC*. The sgRNA sequence for *MED12* ablation was recovered from the genome-wide sgRNA library (sgMED12_4: TTCACATTATGACCAACACC) and sgRNA reagents were obtained from Integrated DNA Technologies, Inc. (6828 Nancy Ridge Drive San Diego, California 92121). CRISPR targeting of the *ARIH2* and *CCNC* loci was performed using multi-guide reagents (*ARIH2* guide_#1: AGACGACCCUGGGGACAUAG, *ARIH2* guide_#2: CUGGUACUCCUCGGGAUCAA, *ARIH2* guide_#3: GGGGUCUGACAGCAAUGAAG; *CCNC* guide_#1: AUUGGUUCAAAUUGUAUAGU, *CCNC* guide_#2: AGAGAAACUUUAAA UCCUUU, *CCNC* guide_#3: UUCUAGUUUGCAAUGGAUUU) from EditCo Bio, Inc. (600 Saginaw Drive Redwood City, CA 94063).

In brief, CRISPR ribonucleoproteins (RNP) were formed by complexing Cas9 (61μM; Alt-R™ S.p. Cas9 Nuclease V3, Integrated DNA Technologies, Cat# 1081059) with sgRNA (100μM; Integrated DNA Technologies) in the presence of Lonza P3 Primary buffer (P3 Primary Cell 4D-Nucleofector X Kit L, Lonza into, Cat# V4XP-3024) at a 0.3:0.22:0.48 ratio and incubating for 20 min at room temperature. Batches of $1x10^7$ NK cells were collected, washed, pelleted, and resuspended in 10μL Cas9-RNP together with 80μL P3 buffer and 10μL electroporation enhancer (100μM; Alt-R™ Cas9 Electroporation Enhancer, Integrated DNA Technologies, Cat#

1075916) for final concentrations of 2.2μM sgRNA, 1.83μM Cas9 and 10μM electroporation enhancer. Electroporation was carried out using the Lonza Bioscience X unit L kit Nucleocuvettes applying the CM137 pulse code. Immediately after electroporation, NK cells were recovered by adding 500μL of prewarmed NK cell medium to the cuvettes and incubated at 37C for 10-15 minutes. Afterwards, NK cells were transferred to cell culture flasks containing prewarmed NK cell medium and irradiated uAPC feeder cells at a NK:uAPC ratio of 1:2 in the presence of IL-2 (200U/mL).

Assessment of sgRNA performance

CRISPR/Cas9-RNP-mediated disruption of targeted genes was verified either by Sanger sequencing paired with sequence trace decomposition via TIDE algorithm[67] or via western blotting. In brief, genomic regions surrounding targeted CRISPR cleavage sites were amplified by PCR and sequenced by Sanger sequencing. Sequencing traces were subsequently decomposed by TIDE algorithm to assess indel frequencies of CRISPR-edited NK cells compared to Cas9 mock-electroporated controls. Mock-electroporated controls were electroporated using the same Cas9 concentration, buffer and electroporation settings but did not receive a targeting guide RNA.[67] The following PCR primers were designed using NCBI Primer-BLAST tool to amplify genomic regions surrounding CRISPR cleavage sites of *MED12*[79]*:* sgRNA_3 FWD: TGCCCTAGTCAGTCTTCCCT, sgRNA_3 REV: AACTTCCCCACCTGAATGGC.

Western blotting

To investigate protein expression from whole cell lysates, NK cells were lysed using IP lysis buffer (Pierce™ IP Lysis Buffer, Thermo Scientific, Cat# 87788) supplemented with protease and phosphatase inhibitors (Halt™ Protease and Phosphatase Inhibitor Single-Use Cocktail, EDTA-Free, Thermo Scientific, Cat# 78443) and incubated for 30 min on ice. Protein concentration was determined using the BCA protein Assay Kit (Pierce) after centrifugation. Cell lysates from indicated experimental conditions were subjected to electrophoresis in equal amounts using SDS-PAGE and transferred to Polyvinyldifluoride membrane (Bio-Rad). Membranes were blocked with 5% milk (in PBST) or 5% bovine serum albumin (BSA, in PBST) for 30 min, followed by incubation with the primary antibody at 4°C overnight. The following primary antibodies were used: ARIH2 (Proteintech, Cat#15006-I-AR), Cyclin C (CST Cat#68179) and b-actin (Sigma-Aldrich, AC-15, Cat# A5441). The membranes were washed three times with PBST (5 min each), and then incubated with secondary antibody (5% milk in PBST) for 60 min. Protein signal was detected by ECL (Amersham) following the vendor's instructions. Densitometry analyses were performed by evaluating band intensity mean gray value of the indicated protein and normalizing it with the mean gray value of the corresponding lane's loading control (β-actin) using ImageJ software.

Analysis of published scRNA-seq data sets

Single cell RNA sequencing data was obtained from publicly available data sets[31,33] and re-analyzed to check for expression of top hits from the transcription factor library and genome-wide CRISPR screens in primary human NK cells. Briefly, for the comparison of NK cells from AML (n=8) and healthy donors (n=8), log10-normalized gene expression data was downloaded.[33] Module score was calculated using R package Seurat.[70] For the comparison of NK cells from pan-cancer patients (n=217) and healthy donors (n=5), gene set module score using pseudo-bulked samples was assessed using the web-based tool *single cell RNA-seq Data Visualization and Analysis* (available at http://pan-nk.cancer-pku.cn).[31] Significance of between-group module score difference was assessed by unpaired Mann-Whitney U test or Kruskal-Wallis test depending on sample size.

Generation of anti-CD70 and anti-TROP2 CAR constructs

The CAR construct targeting CD70 (iC9.CD27(ECD).CD28.zeta.2 A.IL-15) referred to as CD27CAR/IL-15 consists of the CD27 extracellular domain (the natural ligand to CD70), coupled to the CD28 costimulatory domain and the CD3ζ signaling domain. Furthermore, it contains iC9 as a safety switch and the IL-15 transgene for autocrine cytokine support and enhanced persistence.

The CAR construct targeting TROP2 (iC9.TROP2scFv (clone hRS7).CD28.zeta.2 A.IL-15) referred to as TROP2CAR/IL-15 incorporates an scFv targeting TROP2 which was derived from the human RS7 sequence of the TROP2-targeting antibody–drug conjugate sacituzumab govitecan), linked with the CD28 costimulatory domain, the CD3ζ signaling domain, an iC9 safety switch and IL-15 cytokine armoring.

Both CAR constructs were cloned into the SFG retroviral backbone. Retroviral supernatant was generated from transfected 293T cells as previously described.[75] CAR transduction efficiency was measured 48-72 hours post transduction by flow cytometry.

NK cell xCELLigence cytotoxicity assays

Human cancer cell lines (CFPAC, OVCAR5, Capan-1 and PATC148) were seeded in 96-well RTCA E-plates (Agilent Technologies, Inc.; Cat# 300601030) one day prior to addition of CRISPR-engineered NK cells. Once NK cells were added at specified E:T ratios, tumor growth was monitored longitudinally reflected in changes in impedance as measured by xCELLigence Real-Time Cell Analysis device (Agilent Technologies, Inc., 5301 Stevens Creek Blvd., Santa Clara, CA 95051, United States). Cytotoxicity data was reported normalized to the time of NK cell addition as normalized cell index. For re-challenge assays, NK cells were harvested, re-counted and added at specified E:T ratios onto new plates containing adherent tumor cells indicated time points (Figure 5A).

Incucyte® live cell killing assays and tumor rechallenge assays

To assess the effects of *MED12* knock-out on shielding NK cells from functional exhaustion, CRISPR-edited NK cells were co-cultured and repeatedly challenged with the cancer cell lines MM1S and MOLM-14 using the Incucyte® live cell imaging (Sartorius).

In brief, CRISPR-edited *MED12* deficient NK cells were co-cultured with MM1S and MOLM-14 cancer cell lines, stably labeled with red fluorescent reporter genes, in 96-well flat clear bottom black microplates (Corning, Cat# 3904) in technical triplicates at an effector-to-target ratio of 1:2. NK cells were re-challenged by adding additional tumor cells at indicated time points. Tumor growth was assessed in real-time as determined using Incucyte® S3 live-cell analysis system (Sartorius AG Otto-Brenner-Str. 20, 37079 Göttingen, Germany). Tumor growth was normalized to time point T0. Killing capacity of CRISPR-perturbed NK cells was normalized to tumor growth, which was set to one.

MED12-deficient CD27CAR/IL-15-NK cells were co-cultured THP-1 cancer cells at indicated E:T ratios and re-challenged by adding additional tumor cells at indicated time points. Tumor growth was normalized to time point T0; NK cell killing was rebased to one at each time of tumor re-challenge.

CRISPR gene-edited *ARIH2*/*CCNC* KO NK cells and non-edited WT controls were co-cultured with Karpas-299 human T cell non-Hodgkin's lymphoma cells stably expressing a red fluorescent reporter gene at indicated E:T ratios and followed longitudinally. NK cells were re-challenged by adding additional tumor cells at indicated time points. Tumor growth was normalized to time point T0.

Incucyte® live-cell spheroid assays

3D spheroids of UM-RC-3, PATC148 and BCX010 human cancer cells were formed by plating 15,000 (PATC148, BCX010) or 20,000 (UM-RC-3) single cells in 50 μL medium in a Corning® 96-well Clear Round Bottom Ultra-Low Attachment Microplate, Individually Wrapped, with Lid, Sterile (Corning, Cat# 7007). The plates were then placed in a 37°C incubator for 24h to allow for the spheroids to form. Once formed, the spheroids were treated with various NK cell conditions in technical duplicate wells or left untreated as controls. Frames were captured with a 4x objective at 4-hr intervals over a number of days. Green signal was quantified using Incucyte® S3 live-cell analysis system (Sartorius) in real-time. Images were exported using the same analysis system. Green signal intensities were normalized to time point T0. NK cell killing was normalized to tumor growth, which was set to one.

Titration of immunosuppressive metabolites

NK cells were cultured together with irradiated uAPC feeder cells in the presence of defined doses of different immunosuppressive metabolites and under hypoxic (O2=1%) conditions. Effects of the immunosuppressive metabolites and hypoxia on proliferation were assessed after 7 days for NK cell culture time and reported normalized to NK cells cultured under normal conditions. Effects on NK cell cytotoxicity were assessed by co-culturing NK cells after 7 days of metabolite exposure with red fluorescent reporter gene-labeled K562 targets in the presence of the specified metabolites and assessing real-time tumor growth through the Incucyte® live cell imaging (Sartorius AG, Otto-Brenner-Str. 20, 37079 Göttingen, Germany).

Mass cytometry (CyTOF) and data analysis

Mass cytometry experiments and primary antibody conjugation were performed as described previously.[89] Briefly, cells were harvested, washed with cell staining buffer (0.5% BSA in PBS) and incubated with 2.5 μM cisplatin (Sigma Aldrich, St Louis, MO) for viability assessment. Cells were washed, incubated with 5 μL of human Fc receptor blocking solution (Trustain FcX, Cat # 422302, Biolegend, San Diego, CA) for 10 min at room temperature, and then stained for cell surface markers with a freshly prepared antibody mix for 30 min at room temperature on a shaker. After washing with cell staining buffer, samples were fixed/permeabilized using BD Cytofix/Cytoperm solution (Cat # 554714, BD Biosciences) for 30 min in the dark at 4°C, washed twice with perm/wash buffer, and stained with antibodies directed against intracellular markers. Samples were then washed and stored overnight in 500 μL of 1.6% paraformaldehyde (EMD Biosciences)/PBS with 125 nM iridium nucleic acid intercalator (Fluidigm). The next day, samples were washed, filtered, counted, and resuspended in MilliQ dH2O supplemented with EQTM four element calibration beads at a concentration of $0.5x10^5$/ml. Samples were acquired on a Helios instrument (Fluidigm) using the Helios 6.5.358 acquisition software (Fluidigm). The antibodies used along with the corresponding metal tag isotopes are as follows: CD45 (Standard Biotools, HI30, 89Y); CCR6 (Miltenyi Biotech, REA190, 141Pr); Eomes (Invitrogen, WD1928, 142Nd); GFP (Biolegend, FM264G, 144Nd); CD8a (Milteny Biotec, REA734, 146Nd); NKG2C (Milteny Biotec, REA205, 147Sm); TRAIL (Milteny Biotec, REA1113, 148Nd); CD25 (Standard Biotools, 2A3, 149Sm); CD69 (Milteny Biotec, REA824, 150Nd); 2B4 (Milteny Biotec, REA122, 167Er); CD95 (Milteny Biotec, REA738, 152Sm); panKIR (R&D systems, 180704, 153Eu); CD27 (Standard Biotools, L128, 155Gd); CX3CR1 (Miltenyi Biotec, REA385, 154Sm); CXCR3 (Standard Biotools, G025H7, 156Gd); OX40 (Milteny Biotec, REA621, 158Gd); CD11c (Standard Biotools, Bu15, 159Tb); Tbet (Standard Biotools, 4B10, 160Gd); TIGIT (Milteny Biotec, REA1004, 152Eu); Ki67 (Standard Biotools, B56, 162Dy); BTLA (Standard Biotools, MIH26, 163Dy); CD73 (Milteny Biotec, AD2, 164Dy); CD160 (Biolegend, BY55, 144Nd); TIM3 (Milteny Biotec, REA635, 165Ho); NKG2D (Standard Biotools, ON72, 166Er); KLRG1 (Milteny Biotec, REA261, 168Er); NKG2A (Standard Biotools, Z199, 169Tm); CD161 (Milteny Biotec, REA631, 170Er); DNAM (Standard Biotools, DX11, 171Yb); PD1 (Milteny Biotec, PD1.3.1.3, 174Yb); PD-L1 (Biolegend, MIH2, 161Dy); LAG3 (Milteny Biotec, REA351, 175Lu); ICOS (Milteny Biotec, REA192, 176Yb); CD16 (Standard Biotools, 3G8, 209Bi); CD57 (Milteny Biotec, REA769, 115In); CD39 (Milteny Biotec, MZ18-23C8, Pt195); Perforin (Standard Biotools, B-D48, Pt196); Granzyme B (Standard Biotools, GB11, Pt198); CD56 (Milteny Biotec, REA196, 106Cd); CD2 (Milteny Biotec, REA972, 111Cd); HLA-DR (Milteny Biotec, REA805, 112Cd); NKp30 (Milteny Biotec, AF29-4D12, 113Cd); NKp46 (Milteny Biotec, REA808, 114Cd); SYK (Biolegend, 4D10.2, 151Eu); ZAP70 (Miltenyi Biotec, REA814, 143Nd); and NKp44 (Milteny Biotec, REA163, 116Cd); 41BB (Standard Biotools, 4B4-1, 173Yb).

Mass cytometry data were analyzed using FlowJo (FlowJo LLC) and OMIQ (Dotmatics). FCS files were first processed using FlowJo by removing beads and then gating singlets in Ir191/193 double positive cells in OMIQ. NK cell populations were identified

Please cite this article in press as: Biederstädt et al., Genome-wide CRISPR screens identify critical targets to enhance CAR-NK cell antitumor potency, Cancer Cell (2025), https://doi.org/10.1016/j.ccell.2025.07.021

by Pt195 (cisplatin)low GFP- hCD45+ CD56^{+} CD3-. The gating strategy was applied to all files. Data from 5,000 NK cell events per condition were randomly subsampled. Normalized data from donors representing the same condition were virtually concatenated. Downstream analysis was performed on randomly sampled 5,000 events from each condition. NK cells from the various conditions were merged to create a single opt-SNE map. The positive population for each marker was gated in OMIQ (Dotmatics). The median expression of each marker was normalized using Z-score, then hierarchically clustered (1-Pearson), and plotted as a heatmap with the percentage positivity overlayed for each marker using Morpheus matrix visualization and analysis software (Broad Institute).

Metabolic assays

The oxygen consumption rate (OCR) was measured using the *Mito Stress Test* or the *XF Substrate Oxidation Stress Test*, using an Agilent Seahorse XFe96 Analyzer (Agilent Technologies, Inc., 5301 Stevens Creek Blvd Santa Clara, CA 95051 United States) per the manufacturer's instructions. Cells were plated in respective media at 250,000 cells per well in a 96-well microplate. Data were analyzed using Wave Software (Agilent Technologies, Inc.).

Multiplex cytokine profiling

For multiplex cytokine profiling using ELISA, supernatants from NK cell and PATC148 co-cultures were harvested at different time points and cytokine and chemokine production was evaluated using Human XL Cytokine Luminex® Performance Assay 46-plex Fixed Panel (R&D Systems, Cat#: LKTM014B). Samples were analyzed using the Millipore MAGPIX instrument (EMD Millipore). Data was acquired using the Luminex xPONENT software and analyzed with Belysa Analysis Software (EMD Millipore). Data were plotted using Morpheus, https://software.broadinstitute.org/morpheus.

Quantitative reverse transcription PCR

To quantify mRNA transcript levels of indicated genes, RNA was extracted from NK cells followed by reverse transcription using *iscript* cDNA Synthesis kit (Bio-Rad, Mylan, Italy). Relative gene expression was assessed using RT-qPCR using the KAPA Probe Fast ABI Prism master mix (Sigma Aldrich; Cat# KK4705). *MED12*, *ARIH2*, *CCNC* and *CISH* Taqman primers (FAM) were purchased from IDT.

GAPDH: Assay IDHs02786624_g1, Catalog# 4331182.
ARIH2: Assay ID: Hs04973086_s1, Catalog# 4351372.
CCNC: Assay ID: Hs01029307_m1, Catalog# 4331182.
CISH: Assay ID: Hs00367082_g1, Catalog# 4331182.
Med12: Assay ID: Hs00326378_m1, Catalog# 4331182.

Relative gene expression levels were assessed compared to the housekeeping gene GAPDH and normalized against non-edited wildtype NK cell controls.

Single-cell RNA sequencing (scRNA-seq)

Gene expression profiling was conducted using scRNA-seq with the 10x Genomics GEM-X Flex for Gene Expression protocol (CG000787). Co-culture experiments were performed by incubating various CRISPR-edited NK cells with the PACTC-148 cell line at an E:T ratio of 4:1. Following a 3-day co-culture period, cells were harvested, counted, and viability was assessed using acridine orange/propidium iodide (AOPI) staining.

A total of 14 samples were collected and fixed using the GEM-X Flex Sample Preparation v2 Kit (10x Genomics, protocol CG000782), following the manufacturer's recommended procedures. Fixed samples were then pooled and multiplexed according to the 10x Genomics multiplexing workflow, enabling simultaneous profiling of multiple conditions in a single GEM-X Flex run. Barcoded single-cell suspensions were loaded onto the Chromium X instrument with a target recovery of 10,000 to 20,000 cells per sample, and library preparation and cDNA amplification were performed using reagents from the GEM-X Flex Gene Expression kit.

Sequencing was performed on the NovaSeq X Plus system using the 10B flow cell with paired end reads, in accordance with the recommended read configuration. Raw sequencing data were processed using Cell Ranger v9, which included sample demultiplexing, alignment to the reference genome, gene expression quantification, and generation of gene-barcode matrices.

Quality control, normalization and integration of scRNA-seq data

Data-cleaning steps were carried out whereby cells not expressing a minimum of 500 molecules and genes expressed by <10 cells were filtered out. Doublets were removed using the SOLO algorithm.[70,80] The data were normalized using log(transformation) for some of the downstream analysis as well as for visualization of gene expression like plots. Quality control, data integration, and the visualization of the gene expression data were performed using Scanpy.[81] For analysis using scVI, the raw count data were used. The probabilistic models scVI, as implemented in Scanpy, were used for integration of scRNA-seq data to compensate for batch effects.[82]

Dimensionality reduction, clustering and visualization of scRNA-seq data

We computed the Uniform Manifold Approximation and Projection (UMAP) embedding for visualization using the embedding learned from scVI. Unsupervised clustering was also carried out using the learned embeddings with PhenoGraph and the Leiden algorithm as implemented in Scanpy.

Please cite this article in press as: Biederstädt et al., Genome-wide CRISPR screens identify critical targets to enhance CAR-NK cell antitumor potency, Cancer Cell (2025), https://doi.org/10.1016/j.ccell.2025.07.021

Cell-type annotations and in-depth analysis

All cells were annotated using CellTypist.[83] Marker gene expression analysis was used to validate and correct the annotation from CellTypist. In this experiment, only two types of cells were identified: NK cells and PATC148 tumor cells. To identify the subpopulations of NK cells, we singled out NK cell populations and conducted follow-up sub-clustering using Seurat (https://satijalab.org/seurat/).[84] In addition, the Scillus (https://github.com/xmc811/Scillus) R package was used for enhanced processing and visualization of scRNA-seq data. The SCPA R package[85] was used to conduct pathway analysis in scRNA-seq data. Pathway activity was defined as a change in multivariate distribution of a given pathway across conditions. All of the figures were plotted either using the functions provided by the above software or using the custom-designed code written in R (version 4.4.2) or Python (version 3.11).

Animal experiments

For the orthotopic mouse model of human pancreatic cancer, NSG mice underwent surgical orthotopic implantation of 3e5 PATC148 cells directly into the pancreas. One week later, mice were treated intraperitoneally with 1e7 cells of indicated NK cell products or left untreated. Flow cytometry analysis of NK cell kinetics was conducted by drawing blood on day 10 post NK injection. To investigate the migration and infiltration of NK cells into tumor beds, mice were euthanized on day 17 post NK cell treatment. Previously, NK cells were harvested from spleen and intraperitoneal fluid for CyTOF analysis to investigate phenotypic alterations of CRISPR-edited NK cells *in vivo*. Pancreases were harvested, fixed and paraffin embedded. Tumor nodules were quantified after hematoxylin and eosin (H&E) staining by an independent pathologist. Immunohistochemistry (IHC) staining for hCD45 and granzyme B was performed on pancreas sections to identify NK cells and cytotoxic NK cells, respectively. Whole slide digital imaging was performed using an Aperio AT2 after immunohistochemical staining on a Leica Bond RX autostainer for CD45 and granzyme B on adjacent serial sections. Images were deconvoluted in HALO v. 3.6 Deconvolution module v.1.1.8. Deconvoluted images were subsequently registered and fused using the same HALO software.

For the luciferase-labeled orthotopic PATC148 pancreatic cancer model, NSG mice underwent surgical orthotopic implantation of 3e5 firefly-luciferase-labelled PATC148^{FFLuc+} cells directly into the pancreas. Seven days later, mice were injected with 5e6 of CRISPR-perturbed NK cells intraperitoneally and corresponding wildtype controls or left untreated. Evaluation of tumor growth was conducted using bioluminescence imaging at indicated time points until saturation. For the systemic multiple myeloma model, NK cells were infused with 3e5 MM1S human multiple myeloma cells and treated with indicated NK cell products seven days later by tail vein injection. NK cell expansion was monitored using flow cytometry by drawing blood on day 10 post NK cell infusion. Mice were followed for body weight and survival.

QUANTIFICATION AND STATISTICAL ANALYSIS

Statistical analyses were conducted with GraphPad Prism (Prism 10.4.0; GraphPad Software Inc.). Quantitative differences were assessed using either ANOVA or Kruskal-Wallis for multiple groups or a t-test and Mann-Whitney U test for two groups. Statistical significance was defined as $P < 0.05$. Mean values ± SD were used to represent the data, unless otherwise specified. The specific statistical tests employed and corresponding sample sizes (n) are detailed in each figure legend.